Journal of Magnetic Resonance 198 (2009) 57–72

Contents lists available at ScienceDirect

Journal of Magnetic Resonance

journal homepage: www.elsevier.com/locate/jmr

Effects of jump dynamics on solid state nuclear magnetic resonance line shapes and spin relaxation times

Robert L. Vold [a,*], Gina L. Hoatson [b]

[a] Department of Applied Science, The College of William and Mary, Small Hall Rm 316A, Campus Drive, Williamsburg, VA 23187-8795, USA
[b] Department of Physics, The College of William and Mary, Small Hall Rm 316A, Campus Drive, Williamsburg, VA 23187-8795, USA

ARTICLE INFO

Article history:
Received 10 November 2008
Revised 12 January 2009
Available online 19 January 2009

Keywords:
Jump dynamics
Deuteron quadrupole echo
Line shape
Relaxation times
Simulation
High spin quadrupoles

ABSTRACT

This paper describes EXPRESS (*EX*change Program for *RE*laxing *S*pin *S*ystems), a computer program that simulates the effects of Markovian jump dynamics for a wide variety of solid state nuclear magnetic resonance experiments. A graphical interface is described that facilitates the definition of rotational jumps around non-commuting axes that may occur at arbitrary, different rates. Solid state deuteron NMR is widely used to investigate such processes, and EXPRESS allows simulations of deuteron quadrupole echo and magic angle spinning line (MAS) shapes, as well as partially relaxed line shapes for measurements of anisotropic relaxation of Zeeman and quadrupolar order. Facilities are included for chemical shift tensors (at user-defined orientations relative to the quadrupole coupling tensors), so that EXPRESS is potentially useful for studies of paramagnetic systems where these interactions are of comparable magnitude. Many of the same techniques used for deuterons can be extended to half-integer quadrupolar nuclei. The same interface that specifies rotational "sites" for deuteron NMR studies is usable in EXPRESS to simulate static line shapes, MAS line shapes, and multiple pulse Carr–Purcell–Meiboom–Gill (CPMG) line shapes for the central transition of high spin quadrupoles with second order quadrupole coupling and chemical shift anisotropy. Representative simulations are displayed that show effects of slow libration on deuteron quadrupole echo line shapes and relaxation time anisotropies. EXPRESS is also used to investigate fundamental differences in the mechanism of echo formation in deuteron MAS and quadrupole CPMG experiments, and to illustrate significant differences between these techniques in the context of high spin quadrupolar nuclei. The program is modular and platform-independent, with facilities for users to add routines for experiments not yet envisioned.

1. Introduction

Nuclear magnetic resonance (NMR) has long been used to investigate rotational motion in solids, on timescales set by the magnitude of orientation-dependent, single-particle spin interactions such as chemical shift anisotropy [1] and quadrupole coupling [2,3]. Deuteron NMR has emerged as a premier technique for quantitative studies, in part because the dominant (first order quadrupole) interaction is both small enough to be experimentally tractable and large enough to provide a wide kinetic window [4]. Artifact-free line shapes can be obtained by the well known quadrupole echo experiment [5,6,2], and the experimentally accessible kinetic window (rates between $\sim 10^4$ and 10^7 s^{-1}) can be extended by several orders of magnitude on the low end by measuring the decay of quadrupole order (aka, spin alignment) [7,8], and on the high end by measuring the orientation dependence of individual spectral densities that govern relaxation of Zeeman (T_{1Z}) and quadrupole (T_{1Q}) order [9,10]. More recently, the advent of commercially available magic angle spinning (MAS) probes capable of stable, high speed spinning (>20 kHz), variable temperature operation combined with significant advances in computational power, make magic angle spinning an attractive alternative to measurements of quadrupole echo line shapes [11–15]. There is a growing awareness [16,17] that many of the same techniques developed in the context of deuteron NMR can be extended to the more complicated arena of half-integer quadrupoles, where line shapes of the central transition are governed by a combination second order quadrupole coupling and chemical shift anisotropy.

A common feature shared by all these NMR techniques is the description of rotational motion by a specific model, and fitting the model to experimental data by adjusting parameters that represent the rates and detailed trajectories of motion. One class of models, widely used to describe motional effects in electron spin resonance (especially of liquid crystals and other ordered fluids) is based on solving the stochastic Liouville equation for (anisotropic) rotational diffusion in presence of an anisotropic pseudopotential [18–22]. This approach is effective for systems in which the multidimensional potential energy surface that governs the motion has low barriers and wide valleys, but is less appropriate for highly con-

* Corresponding author. Fax: +1 757 221 3540.
E-mail address: rlvold@wm.edu (R.L. Vold).

1090-7807/$ - see front matter © 2009 Elsevier Inc. All rights reserved.
doi:10.1016/j.jmr.2009.01.008

strained environments such as molecular crystals. In the latter case, it is plausible to describe the motion by sudden (Markovian) jumps among a number of discrete orientational "sites". In this context, specifying a motional model amounts to defining the number, relative orientations, and relative populations of the sites as well as which sites are to be "connected" by jumps at specified rates.

Simulating the effects of intermediate time scale dynamics on NMR experiments is a daunting task. For all but the very simplest motional models, numerical solution of coupled sets of ordinary differential equations is required, and the problem is compounded for polycrystalline or amorphous materials by the need to sum the solutions over hundreds or thousands of crystallite orientations. General purpose programs for simulating deuteron quadrupole echo line shapes for discrete jumps among *N-sites* have long been available [23,24]. The multi-axis jump formalism of Greenfield et al. [23] has been extended using procedures described by Griffin et al. [25] to simulate experiments designed to measure anisotropic T_{1Z} [26] and more recently, T_{1Q} [27,28]. However, these programs rely extensively on obsolete FORTRAN code and are difficult to modify for simulations of more modern experiments such as magic angle spinning. Programs designed to simulate effects of motion for specific experiments and relatively simple *N*-site jump models have been described in the literature [11,29–32,13,33,34,14,16,35,15,17,36] but we are unaware of any program that can simulate effects of intermediate time scale dynamics on all of the experiments mentioned above.

This paper describes an *Ex*change *P*rogram for *Re*laxing *S*pin *Sy*stems, EXPRESS, that provides a common interface for simulating effects of motion on all types of pulsed NMR experiments. Coded in MATLAB, it is platform-independent and easy to modify. While not fully optimized for computational efficiency, direct comparisons with equivalent hand coded FORTRAN or C routines shows that EXPRESS code typically runs 2–4 times faster than compiled code similar to that used in the QE line shape program MXQET [23]. The program features a graphical user interface (GUI) with on-line help features, designed to make it more readily accessible to non-specialists in the art of slow motion simulations. In Section 2 we present the theory and algorithms used in EXPRESS, including a discussion of multi-axis jump dynamics and the tensor conventions used for chemical shift anisotropy, first order quadrupole, and second order quadrupole interactions. In Section 3 we illustrate features of the GUI and discuss problems related to the plethora of parameters that arise in complex multi-site motional models. In Section 4 we illustrate typical applications of EXPRESS by using it to analyze several features of multi-axis jump motion for deuteron systems, and to investigate theoretical problems that arise with motion of half-integer, high spin quadrupolar nuclei.

2. Theory

2.1. Stochastic Liouville formalism

EXPRESS simulates NMR line shapes and relaxation times by solving the stochastic Liouville equation for the spin density matrix, where motion is incorporated as discrete Markovian jumps. Thus, if $\rho_j(t) = \rho(\Omega_j, t)$ stands for the (reduced) density matrix for spins in a molecular fragment specified at time t by a set of Euler angles $\Omega_j = (\alpha_j, \beta_j, \gamma_j)$ with respect to a molecule-fixed reference frame, EXPRESS describes the time evolution of in terms of jumps between N discrete orientational sites $j,k,l,\ldots$:

$$\frac{d\rho^{(j)}}{dt} = i[\rho^{(j)}, H^{(j)}(t)] + \sum_{k=1}^{N} \frac{P(j,k)\rho^{(j)}P(j,k) - \rho^{(j)}}{\tau_{jk}} \tag{1}$$

Here, $H^{(j)}(t)$ is the Hamiltonian for interactions between spins in orientational site j among themselves and with their surroundings, P(j,k) is a permutation operator that interchanges the site labels j and k, and $k_{jk} = 1/\tau_{jk}$ is defined as the average rate of jumps from site k to site j (note the order of the subscripts). The sites may have unequal populations at thermal equilibrium, and the forward and reverse rates are then related by the principle of microscopic reversibility, $p_k k_{jk} = p_j k_{kj}$, where p_j is the population of site j.

In its present form, EXPRESS considers only a small subset of the density matrix elements implicit in Eq. (1). In absence of rf fields, $H^{(j)}(t)$ becomes time independent (in the rotating frame). The time dependence of transverse magnetization, needed to compute line shapes for stationary and/or rotating samples, is then obtained from the subset of density matrix elements corresponding to 1-quantum coherence in each site. Thus if the vector $m_j = [\rho^{(j)}_{pq}(t), \rho^{(j)}_{rs}(t), \rho^{(j)}_{tu}(t)\ldots]$ represents the 1-quantum coherences in site j, the relevant subset of density matrix elements is Eq. (1) is governed by the equations

$$\frac{d}{dt}\begin{bmatrix} m^{(1)} \\ m^{(2)} \\ \vdots \\ m^{(N)} \end{bmatrix} = i\begin{bmatrix} \Omega^{(1)} & 0 & 0 & 0 \\ 0 & \Omega^{(2)} & 0 & 0 \\ 0 & 0 & \ldots & 0 \\ 0 & 0 & 0 & \Omega^{(N)} \end{bmatrix}\begin{bmatrix} m^{(1)} \\ m^{(2)} \\ \ldots \\ m^{(N)} \end{bmatrix} + \begin{bmatrix} k_{11}I & k_{12}I & \ldots & k_{1n}I \\ k_{21}I & k_{22}I & \ldots & k_{2n}I \\ \vdots & \vdots & \cdots & \vdots \\ 0 & k_{n2}I & \mathrm{L} & k_{nn}I \end{bmatrix}\begin{bmatrix} m^{(1)} \\ m^{(2)} \\ \vdots \\ m^{(N)} \end{bmatrix} = A\begin{bmatrix} m^{(1)} \\ m^{(2)} \\ \vdots \\ m^{(N)} \end{bmatrix} \tag{2}$$

where I is the $N \times N$ identity matrix and $k_{jj} = \sum_{k\neq j,1}^{N} k_{kj}$. The $\Omega^{(j)}$ in Eq. (2) are diagonal matrices, whose elements are the corresponding 1-quantum precession frequencies for site j. When *rf* fields *are* present, the first term of Eq. (1) mixes coherences of different order and it would be necessary to expand Eq. (2) to include all density matrix elements, diagonal and off-diagonal. The solution is then practical only in the simplest cases [37], and is beyond the purview of EXPRESS.

EXPRESS can simulate partially relaxed line shapes for Zeeman relaxation (T_{1Z}) and relaxation of quadrupole order (T_{1Q}), but only for spin $I = 1$. In this case only, Zeeman order $M_Z^{(j)}(t)$ and quadrupole order $Q_Z^{(j)}(t)$ associated with site j are given by

$$\begin{aligned} M_Z^{(j)}(t) &= \rho_{11}^{(j)}(t) - \rho_{33}^{(j)}(t) \\ Q_Z^{(j)}(t) &= \rho_{11}^{(j)}(t) - 2\rho_{22}^{(j)}(t) + \rho_{33}^{(j)}(t) \end{aligned} \tag{3}$$

where the spin eigenstates are $|1\rangle = |+\rangle$, $|2\rangle = |0\rangle$, and $|3\rangle = |-\rangle$ respectively. In *absence* of jumps between orientational sites, $M_Z^{(j)}(t)$ and $Q_Z^{(j)}(t)$ for each site, j, would evolve independently in time according to the relations:

$$\begin{aligned} M_Z^{(j)}(t) &= M_Z^{(j)}(\infty) + e^{-R_{1Z}^{(j)}t}\left(M_Z^{(j)}(0) - M_Z^{(j)}(\infty)\right) \\ Q_Z^{(j)}(t) &= e^{-R_{1Q}^{(j)}t}Q_Z^{(j)}(0) \end{aligned} \tag{4}$$

where the relaxation rates R_{1Z} and R_{1Q} of Zeeman and quadrupolar order are given by

$$\begin{aligned} R_{1Z}^{(j)} &= \frac{1}{T_{1Z}^{(j)}} = \frac{3\pi^2}{2}\left(C_Q^{(j)}\right)^2\left[J_1^{(j)}(\omega_0) + 4J_2^{(j)}(2\omega_0)\right] \\ R_{1Q}^{(j)} &= \frac{1}{T_{1Q}^{(j)}} = \frac{9\pi^2}{2}\left(C_Q^{(j)}\right)^2 J_1^{(j)}(\omega_0) \end{aligned} \tag{5}$$

The spectral density functions, $J_1^{(j)}(\omega_0)$ and $J_2^{(j)}(2\omega_0)$, refer to rapid motions *entirely within* site (j), over which $H^{(j)}(t)$ in Eq. (1) is assumed to be averaged.

In principle, the Markovian jumps included in Eq. (1) then couple the time evolution of $M_Z^{(j)}(t)$ to that of $M_Z^{(k)}(t)$ (but not to $Q_Z^{(k)}(t)$). When the jump rates are large compared with the difference in the intrinsic site-dependent relaxation rates,

$$k_{jk} \gg \left| R^{(j)}_{1Z,1Q} - R^{(k)}_{1Z,1Q} \right| \tag{6}$$

then the Zeeman and quadrupolar order in each site relaxes (independently) at the same average rate $\langle R_{1Z}\rangle$ and $\langle R_{1Q}\rangle$, respectively. Slower motions can profitably be studied by one or two dimensional saturation transfer experiments. Currently EXPRESS does *not* simulate such experiments. Instead, it makes the implicit assumption that Eq. (6) is always valid (even though the user can enter the value zero for any desired jump rate), and ignores the intrinsic relaxation rates (Eq. (5)) in comparison to spin lattice relaxation induced directly by the sudden orientational jumps from site to site. It then follows that the relaxation of Zeeman and quadrupole order associated with each site (whether or not the corresponding 1-quantum precession frequencies are motionally averaged) is given by dropping the now irrelevant site label superscript (j) from Eqs. (3) and (4).

In many cases of practical interest, the quadrupole coupling constants (and asymmetry parameters) may change from site to site. In most previous formulations, this phenomenon was taken into account (usually implicitly) by averaging $(C^{(j)}_Q)^2$ in Eq. (5) over the sites connected by jumps. This incorrect procedure fails to account, for example, for relaxation of a quadrupolar nucleus that jumps from a liquid site with $C_Q = 0$ to an asymmetric site in a solid where C_Q is non-zero. EXPRESS includes the site-dependent quadrupole coupling parameters as part of the Hamiltonian, which are assumed to switch randomly (at average rate k_{jk}) between sites j and k. Thus, EXPRESS simulates the time evolution of diagonal density matrix elements for each site according to Eqs. (3) and (4), with relaxation rates given by

$$\begin{aligned} R^{(j)}_{1Z} &= 1/T^{(j)}_{1Z} = J_1(\omega_0) + 4J_2(2\omega_0) \\ R^{(j)}_{1Q} &= 1/T^{(j)}_{1Q} = 3J_1(\omega_0) \end{aligned} \tag{7}$$

where it can be shown that the spectral densities $J_M(M\omega_0)$ are given by weighted sums of at most $N-1$ Lorenztian functions of the form $A_k\lambda_k/(\lambda_k^2 + M^2\omega_O^2)$, where the λ_k are the non-zero eigenvalues of the kinetic matrix $K = \{k_{jk}\}$. The weighting factors A_k are messy functions of the eigenvectors of K and the site orientation angles, and include cross products of the form $C^{(j)}_Q C^{(k)}_Q$.

For spin $I = 1$, the relaxation time T_{1Q} of quadrupole order due to jump motion is determined exclusively by a single spectral density function, $J_1(\omega_0)$. When the correlation time(s) for jump motion are short enough to yield significant contributions to this spectral density, measurements of the anisotropy of T_{1Q} (for example, by means of broad band Jeener–Broekaert excitation [38]) can profitably be combined with T_{1Z} anisotropy to determine the orientation dependence of both spectral densities. EXPRESS simulates (ideal) broadband Jeener–Broekaert excitation simply by initial inversion of one half of the powder pattern. If this is not achieved in practice (and it never is), the simulated partially relaxed line shapes should *not* be matched to experimental ones, because the experimental initial excitation profile will never match the simulated one. However, it is still entirely possible to fit corresponding points on the simulated and experimental line shapes to exponential recovery curves, and match the corresponding relaxation rates to determine the anisotropy of $J_1(\omega_0)$. This procedure is illustrated in Section 3.

2.2. Multi-axis jump processes

EXPRESS addresses a broad range of N site problems, for which the site orientations are specified in terms of sets of successive rotations. The *first* rotation, $\Omega^{(1)}_j = (\alpha^{(1)}_j, \beta^{(1)}_j, \gamma^{(1)}_j)$, rotates the principal axis system for the relevant interaction tensor into coincidence with an intermediate jump frame, F_1. N_1 such rotations can be specified, $j = 1,2,\ldots N_1$. The connectivity of these sites is specified by $N_1(N_1-1)/2$ independent, non-zero entries of a kinetic matrix K_1. In many cases, a single rate constant suffices to describe these jumps. For example, 3-fold hops of a methyl group about its C_3 axis are described by the matrix $K_1 = k_3\begin{pmatrix} -2 & 1 & 1 \\ 1 & -2 & 1 \\ 1 & 1 & -2 \end{pmatrix}$. A *second* rotation, $\Omega^{(2)}_k = (\alpha^{(2)}_k, \beta^{(2)}_k, \gamma^{(2)}_k)$, may then be defined to rotate the intermediate jump axes into any of N_2 different orientations with respect to a molecule-fixed reference frame. For example, librational motion of the methyl C_3 axis defined above might be modeled by jumps among 4 sites that define the boundary of a narrow cone, with corresponding K-matrix $K_2 = k_{cone}\begin{pmatrix} -3 & 1 & 1 & 1 \\ 1 & -3 & 1 & 1 \\ 1 & 1 & -3 & 1 \\ 1 & 1 & 1 & -3 \end{pmatrix}$ or alternatively, $K_2 = k_{cone}\begin{pmatrix} -3 & 1 & 1 & 1 \\ 1 & -1 & 0 & 0 \\ 1 & 0 & -1 & 0 \\ 1 & 0 & 0 & -1 \end{pmatrix}$. In both these examples, there are 12 sites but only two independent jump rates.

A well known theorem states that the product of any two rotations is also a rotation. Thus, the set of N_1N_2 sites defined by the double rotation $\Omega^{(2)}\Omega^{(1)}$ can equally well be described by specifying N_1N_2 values for a single, composite rotation. It should be noted that the order in which the rotations are performed is important; $\Omega^{(2)}\Omega^{(1)}$ is not the same as $\Omega^{(1)}\Omega^{(2)}$. EXPRESS allows users to enter site orientation angles and jump rates frame by frame, and automatically computes and displays the equivalent one-frame representations of site orientations and jump rates prior to computing the time evolution of relevant single quantum coherences.

2.3. Conventions for Euler angles

Since EXPRESS simulates the effects of jump dynamics on a wide variety of NMR experiments involving many different interactions, it is particularly important that definitions and conventions with regard to tensor interactions, principal components, Euler angles, etc. be clearly stated and consistently used.

Few topics in NMR offer more opportunities for confusion than the conventions used to describe the rotations needed to describe tensor interactions in various coordinate systems. EXPRESS is based on Rose conventions [39,40]; the user is warned that these differ from those of Edmonds [41] or Goldstein [42]. In particular, if $R(\alpha,\beta,\gamma)$ is the operator that rotates the Principal Axis System (*PAS*) of a particular Cartesian tensor into coincidence with a reference frame fixed in the laboratory, EXPRESS makes use of the following matrix representation:

$$\begin{aligned} R(\alpha,\beta,\gamma) &= e^{-i\alpha I_Z} e^{-i\beta I_Y} e^{-i\gamma I_Z} \\ &= \begin{pmatrix} \cos\alpha & -\sin\alpha & 0 \\ \sin\alpha & \cos\alpha & 0 \\ 0 & 0 & 1 \end{pmatrix} \\ &\quad \times \begin{pmatrix} \cos\beta & 0 & \sin\beta \\ 0 & 1 & 0 \\ -\sin\beta & 0 & \cos\beta \end{pmatrix} \begin{pmatrix} \cos\gamma & -\sin\gamma & 0 \\ \sin\gamma & \cos\gamma & 0 \\ 0 & 0 & 1 \end{pmatrix} \end{aligned} \tag{8}$$

This operator describes a rotation first through angle γ about the *PAS z-axis*, then through angle β about the *original* (*PAS*) y-axis and finally by angle α about the *original* (*PAS*) z-axis. As discussed by Brink and Satchler [40, p. 20], this same rotation is obtained by first rotating through angle α about the *PAS z-axis*, then through angle β about the new (intermediate) y-axis, and finally through angle γ about the next (second intermediate) z-axis. The first sequence is easier to visualize, but both give the same result.

It is not entirely trivial to determine the actual Euler angles, (α,β,γ), for the single rotation that is equivalent to $R(\alpha_1,\beta_1,\gamma_1)$ followed by $R(\alpha_2,\beta_2,\gamma_2)$. One way to do this is to construct the two individual matrices R_1 and R_2 using Eq. (8), then compute their product $R = R_1R_2$ numerically, perform the three multiplications specified in Eq. (8) analytically to obtain corresponding algebraic expressions for individual elements of the composite rotation matrix, and the resulting equations to obtain the desired angles. For example, R_{33} turns out to be just $\cos(\beta)$, so that β for the composite rotation is just $\cos^{-1}[(R_1R_2)_{33}]$. In MATLAB, the ACOS function returns angles between zero and π (radians), while the ASIN function returns values between $-\pi$ and $+\pi$. Considerable care is needed to ensure that the Euler angles α and γ are defined instead on the conventional interval $0 \leqslant (\alpha,\gamma), \leqslant 2\pi$.

Each orientational site within a given jump frame is specified by Euler angles (α,β,γ) for the rotation that rotates the coordinate axes for this site into coincidence with the reference axes of the next frame. This process begins with the Principal Axis System (*PAS*) for the EFG tensors (for experiments involving spin $I > 1/2$) or CSA tensors (for $I = 1/2$). It is important to note the "direction" of the rotations: *PAS* → *(intermediate frame(s))* → *crystal-fixed* (or rotor fixed) axes. Each rotation is specified with respect to axes fixed in the frame *from which it starts*.

2.4. Conventions for tensor interactions

The Hamiltonian operator for a spin in a solid sample, placed in a strong, constant magnetic field $\vec{B} = B_0\hat{z}$, can be written in terms of the Zeeman part, $H_0/\hbar = -\omega_0 I_Z = -\gamma B_0 I_Z$, and a sum of terms that account for all the relevant spin interactions. The universal NMR convention [43] calls for frequencies to increase towards the *left*. The natural units of H (more precisely, $H/\hbar$) are radians/sec, *not* hertz, kilohertz, or ppm. Thus, if ω is a typical frequency, the quantity ωt (in radians) is dimensionless when time t is expressed in seconds. Motional rates, k, are specified in inverse seconds, s^{-1}, so that kt is also a dimensionless quantity. It is both confusing and incorrect to refer to jump rates in "hertz" or "kilohertz"—one hertz is 2π times one inverse second. In EXPRESS, frequencies entered as hertz, kilohertz, or ppm are converted internally to radians/sec before being used in any computations, in order to minimize the chance of unit conversion errors. Rates are entered in units of inverse seconds, s^{-1}.

EXPRESS deals with chemical shift anisotropy, first order quadrupole, and second order quadrupole interactions. The number of different conventions appearing in the literature on these interactions is second only to the number of different conventions used to define Euler angles. Unfortunately, this makes it rather difficult to compare simulations performed with different programs. We offer no solution to this problem, other than to state as clearly as possible the following definitions that are used in EXPRESS. The Hamiltonian operator can be written as the following sum of terms:

$$H = H_Z + H_{CS} + H_Q \tag{9}$$

where

$$\begin{aligned} H_Z &= -\omega_0 I_Z = -\gamma B_0 I_Z \\ H_{CS} &= \sum_{L=0}^{2}\sum_{M=-L}^{L}(-1)^M R_{L,M}^{(CS)} T_{L,-M}^{(CS)} \\ H_Q &= \sum_{L=0}^{2}\sum_{M=-L}^{L}(-1)^M R_{L,M}^{(Q)} T_{L,-M}^{(Q)} \end{aligned} \tag{10}$$

Here, the $T_{L,M}$ are spherical irreducible tensor spin operators and the $R_{L,M}$ are orientation-dependent functions of the relevant interaction strengths (not to be confused with the rotation matrices discussed in the preceding section). Eq. (10) is valid in any coordinate system. For convenience in calculating the spin response, it is usual to focus on laboratory fixed coordinates (along B_0 along Z).

2.5. Quadrupole coupling

In this case, the $T_{L,M}$ are given for the quadrupole interaction by

$$\begin{aligned} T_{0,0}^{(Q)} &= T_{1,0}^{(Q)} = T_{1,\pm1}^{(Q)} = 0 \\ T_{2,0}^{(Q)} &= \frac{1}{\sqrt{6}}(3I_Z^2 - I\cdot I) \\ T_{2,\pm1}^{(Q)} &= \mp\frac{1}{2}(I_Z I_\pm + I_\mp I_Z) \\ T_{2,\pm2}^{(Q)} &= \frac{1}{2}I_\pm^2 \end{aligned} \tag{11}$$

The $L = 0$ and $L = 1$ tensors in these expressions are not really zero, but they vanish exactly from the Hamiltonian in Eq. (10) because the electric field gradient tensor, which appears in the corresponding $R_{L,M}^{(Q)}$ terms, is symmetric and has zero trace. Thus, only the $L = 2$ terms survive, and we may write

$$R_{2,M}^{(Q)}(LAB) = \sum_{K=-2}^{2} R_{2,K}^{(Q)}(PAS) D_{K,M}^{(2)}(\alpha_Q(t),\beta_Q(t),\gamma_Q(t)) \tag{12}$$

Here, the time independent quantities $R_{2,K}^{(Q)}(PAS)$ are given by

$$\begin{aligned} R_{2,0}^{(Q)}(PAS) &= \sqrt{3/2}\left(\frac{e^2 Q q_{ZZ}}{2I(2I-1)\hbar}\right) \\ &= \sqrt{3/2}\left(\frac{2\pi C_Q}{2I(2I-1)}\right) = \sqrt{3/2}\,\omega_Q \\ R_{2,\pm1}^{(Q)}(PAS) &= 0 \\ R_{2,\pm2}^{(Q)}(PAS) &= \frac{1}{2}\omega_Q\eta_Q \\ \eta_Q &= \frac{q_{XX}-q_{YY}}{q_{ZZ}} \end{aligned} \tag{13}$$

The quantities eq_{XX}, eq_{YY}, and eq_{ZZ} are the principal components of the electric field gradient (EFG) tensor. Early practitioners of nuclear quadrupole resonance [44] established the now universally accepted convention that the axis of the numerically largest EFG component is labeled Z, and the other two axes labeled such that the asymmetry parameter, η_Q, is restricted to the range $0 \leqslant \eta_Q \leqslant 1$. Many authors interchange the definition used here in Eq. (13) for X and Y. Formulae derived by those authors differ from those used in EXPRESS by changing the sign of terms that depend on odd powers of η_Q. Occasionally, papers may be found with η_Q defined as in Eq. (13), but with $R_{2,\pm2}^{(Q)}(PAS)$ defined as $-\omega_Q\eta_Q/2$. In those papers, no sign change need be made for comparison with EXPRESS formulae. This lack of consistent notation may be called "migration of signs". Unfortunately, the literature is also replete with migration of the mysterious numerical factors, e.g., $(-1)^M$, $\sqrt{1/6}$, ±1/2, $\sqrt{3/2}$, etc that appear in Eqs. (11)–(13): they tend to be partitioned differently by different authors between the tensor spin operators $T_{L,M}$ and the corresponding lattice functions $R_{L,-M}$. However, the partitioning of the numerical factors is NOT completely arbitrary. In particular, the numerical factors displayed in Eq. (4) for the tensor operators arise from their definition as a normalized, irreducible representation of the full rotation group and if this normalization is not used, then the basic transformation equation, Eq. (5), is no longer valid. Finally, some authors refer to ω_Q as "the quadrupole coupling constant", and others may define ω_Q to be three time larger than implied by Eq. (13). Note also the use of $\hbar$ in Eq. (13); the quadrupole coupling constant, $C_Q = e^2 Q q_{ZZ}/h$, has units of Hz. Despite these difficulties, there is by now almost universal agreement that the fundamental quantities measured by NMR should be reported as C_Q (in Hz, kHz, or MHz) and η_Q.

2.6. Chemical shift anisotropy

The chemical shift Hamiltonian is more complicated than the quadrupole Hamiltonian, because the shielding tensor, unlike the EFG tensor, is neither traceless nor symmetric. The expressions used in EXPRESS are entirely consistent with those described in detail by Duer [45]; an abbreviated discussion is presented here.

It is possible to represent any second rank tensor as the sum of a *symmetric* 3×3 matrix and an *antisymmetric*, traceless 3×3 matrix. It can be shown [46,47] that the antisymmetric part of the shielding tensor can contribute to spin lattice relaxation, but it never has any significant effect on the orientation-dependent line shape. The antisymmetric part of the shielding tensor is ignored in EXPRESS line shape simulations. Recognizing that in laboratory coordinates (only!), $\vec{B} = B_0 z$, the relevant terms in Eq. (10) are then given by

$$\begin{aligned} T^{(CS)}_{0,0} &= -\frac{1}{\sqrt{3}} B_0 I_Z \\ T^{(CS)}_{1,0} &= 0 \\ T^{(CS)}_{1,\pm1} &= \frac{1}{2} B_0 I_\pm \\ T^{(CS)}_{2,0} &= \frac{1}{\sqrt{6}}(3 I_Z B_0 - \vec{I}\cdot\vec{B}) = \sqrt{2/3} I_Z B_0 \\ T^{(CS)}_{2,\pm1} &= T^{(CS)}_{2,\pm2} = 0 \end{aligned} \tag{14}$$

and

$$\begin{aligned} R^{(CS)}_{0,0}(LAB) &= -\frac{\gamma}{\sqrt{3}}(\sigma_{11}+\sigma_{22}+\sigma_{33}) \\ R^{(CS)}_{2,M}(LAB) &= \gamma \sum_{K=-2}^{2} R^{(CS)}_{2,K}(PAS) D^{(2)}_{K,M}(\alpha_{CS}(t), \beta_{CS}(t), \gamma_{CS}(t)) \end{aligned} \tag{15}$$

We note in passing that the term $T^{CS}_{00} R^{CS}_{00}$, which is independent of orientation, gives rise to the isotropic chemical shift. If this is site-dependent, it will contribute to the dynamic line shape as computed by EXPRESS.

It is convenient at this point to depart (slightly) from rigorous consistency with the general theory of irreducible tensor operators and drop the minus signs from both T^{CS}_{00} and R^{CS}_{00}, transfer the constant factor B_0 from Eqs. (14), (15), and transfer the factor $\sqrt{2/3}$ from $T^{(CS)}_{2,0}$ in Eq. (14) onto the associated $R^{(CS)}_{2,M}(PAS)$. Since $T^{(CS)}_{2,\pm1} = T^{(CS)}_{2,\pm2} = 0$, this does *not* invalidate the basic transformation expressions. Thus, EXPRESS makes use of the revised definitions

$$\begin{aligned} T^{(CS)}_{0,0} &= 1 \\ T^{(CS)}_{1,0} &= T^{(CS)}_{1,\pm1} = 0 \\ T^{(CS)}_{2,0} &= I_Z \\ T^{(CS)}_{2,\pm1} &= T^{(CS)}_{2,\pm2} = 0 \end{aligned} \tag{16}$$

and

$$\begin{aligned} R^{(CS)}_{0,0}(LAB) &= R^{(CS)}_{0,0}(PAS) = \omega_0 \frac{1}{3}(\sigma_{11}+\sigma_{22}+\sigma_{33}) \\ R^{(CS)}_{2,M}(LAB) &= \sum_{K=-2}^{2} R^{(CS)}_{2,K}(PAS) D^{(2)}_{K,M}(\alpha_{CS}(t), \beta_{CS}(t), \gamma_{CS}(t)) \end{aligned} \tag{17}$$

where now,

$$\begin{aligned} R^{(CS)}_{2,0}(PAS) &= \frac{2}{3}\omega_0\left(\sigma_{33} - \frac{1}{2}(\sigma_{11}+\sigma_{22})\right) = \frac{2}{3}\omega_0 \Delta\sigma \\ R^{(CS)}_{2,\pm1}(PAS) &= 0 \\ R^{(CS)}_{2,\pm2}(PAS) &= \frac{\omega_0}{\sqrt{6}}(\sigma_{11}-\sigma_{22}) = \frac{1}{3}\omega_0 \eta_{cs} \Delta\sigma \end{aligned} \tag{18}$$

Eq. (18) serve to define the chemical shift anisotropy, $\Delta\sigma$, and the associated asymmetry parameter, η_{CS}. In EXPRESS, these quantities (along with the isotropic shift, $\sigma_{iso} = (\sigma_{11}+\sigma_{22}+\sigma_{33})/3$) can be specified for each site. The definitions of $\Delta\sigma$ and η_{CS} are those suggested originally by Haeberlen [47], and are in accord with the most recent IUPAC recommendations [48]. It should be noted that the latter recommendations also allow an alternative definition of $\Delta\sigma$ that is larger than ours by a factor of 3/2.

2.7. Second order quadrupole effects

For half-integer quadrupolar spins $I > 1$, EXPRESS includes second order effects of the quadrupole Hamiltonian, based on the formalism presented by Goldman et al. [49]. In essence, this amounts to starting with a Hamiltonian, $H = H_0 + H_1$, and a known basis $|\psi_0\rangle$ in which H_0 is diagonal, and then deriving a set of operators $H^{(1)}, H^{(2)}, \ldots$ that commute with H_0 and whose matrix representation in the $|\psi_0\rangle$ basis yield well known second order expressions for the eigenstates. The second order quadrupole Hamiltonian is given by:

$$H^{(2)}_Q = -\frac{\omega_Q^2}{\omega_L} \sum_{m>0}^{2} R_{2,m} R_{2,-m} \frac{[T_{2,m}, T_{2,-m}]}{m} \tag{19}$$

where the $T_{2,m}$ are given by Eq. (11) and corresponding $R_{2,m}$ are given by Eqs. (12) and (13). Explicit expressions for the site frequencies of the central transition in terms of C_Q, η, and Euler angles relating *PAS* to lab fixed axes can be found the literature [50,51,16,52]. EXPRESS uses formulae presented in Ref. [51] for simulating powder patterns of non-rotating samples, and formulae given by Zheng et al. [50] for rotating samples.

2.8. Spin lattice relaxation

In its present version, EXPRESS can simulate the effects of jump motion on spin lattice relaxation time anisotropy as monitored by partially relaxed quadrupole echo line shapes or multiple quadrupole echo trains, but only for spin $I = 1$ (e.g., deuterons). The algorithm was first described by Wittebort, et al. [24]. The extension to multi-axis jumps is described in Refs. [26] and [28]. However, in Ref. [26] the correlation functions $\langle R_{2,m}(t) R^*_{2,m}(t+\tau)\rangle$ are all normalized to unity at $\tau = 0$, a procedure which requires that every site has the same C_Q. In earlier programs based on Ref. [26], such as MXQET [23], it was possible to define site-specific C_Q values but when these programs were modified to include spin lattice relaxation, all spectral densities were scaled by the average C_Q. In Eq. (6) above, the C_Q value for each site has been incorporated into the definition of $R_{2,m}(t)$. This makes it possible, for example, to define all sites to have the same *PAS* orientation, but different *values* of C_Q. When one site has $C_Q = 0$, the effect is to simulate spectral densities for exchange between solid and liquid phases. The feature was not available in earlier programs.

In principle, the effects of jump motion on quadrupole relaxation of nuclei with spin $I > 1$ is governed by the same two spectral density functions, $J_1(\omega_0)$ and $J_2(2\omega_0)$, that occur in the formulation for $I = 1$. However, in most experimental situations this is not the dominant process. Instead, relaxation is often found to proceed through modulation of the electric field gradient tensor due to lattice vibrations (formulated as a second order Raman process [53]). Moreover, the recovery functions are sums of exponentials whose relative weights depend in a complicated way on the initial excitation conditions as well as the spin I and the relative magnitudes of $J_1(\omega_0)$ and $J_2(2\omega_0)$. As currently coded, EXPRESS is not sufficiently general to deal with these problems.

2.9. Powder averaging

It is well known that simulations of NMR spectra of solid powders are computationally demanding because they must be repeated for many hundreds or even thousands of different powder orientations. Considerable attention has been paid to this problem in the literature [54]. The general aim is to replace the exact integral over powder orientations by a discrete sum that has the fewest possible terms needed to approximate the exact result within a specified tolerance. It has long been realized that the *least* efficient procedure is to divide the integration interval for each powder orientation angle into a large number of equal intervals. Levitt and coworkers [54] classify the large number of alternative procedures into those based on "geometry", which attempt to construct sets of orientations that define equal solid angles over the unit sphere, and those based on "mathematics" that attempt to annihilate as many higher moments as possible of the function to be integrated, expanded in an appropriate basis set.

Most if not all of the attention paid to this problem in the NMR literature is concerned with simulating the time evolution of the density operator governed by unitary propagators, i.e. without attention to stochastic dynamics. It is not obvious whether any of the commonly used procedures are truly optimal for systems with slow or intermediate time scale dynamics. In part for this reason, EXPRESS offers a choice of tiling schemes. In practice, however, it appears that the commonly used ZCW procedure [55,56] is close enough to optimal that efforts to improve computational efficiency are better spent on improving other numerical tasks.

For all but one experiment dealt with in EXPRESS, it is sufficient to integrate over only two of the three powder angles needed to fully align a crystallite-fixed axis system with laboratory fixed axes (α,β). The one exception is dynamic line shapes for second order quadrupole coupling under MAS or OMAS conditions. In this case, EXPRESS uses full three-angle sets (α,β,γ). Anticipating future advances in defining optimal selection of powder angles, EXPRESS uses a single subprogram for this purpose, that returns different sets of powder angles depending on a user-specified calling option.

3. EXPRESS overview

All the options available in EXPRESS are controlled by a MATLAB graphical interface, shown schematically in Fig. 1. When first invoked, EXPRESS displays a list of default parameters and a set of control buttons, display windows, and parameter input windows. On-line instructions are available by a toggle that activates "help mode", such that clicking on any other control displays an explanation of how to use that particular control but takes no other action. Parameters grouped in the "Experiments" and "Site Definitions" panels can be entered in any order, and can be changed at will before running the simulation. Experiment options currently available in EXPRESS are listed in Table 1.

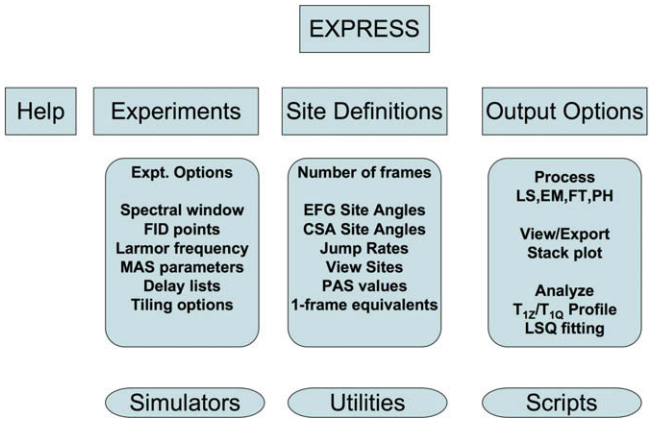

Fig. 1. Overview of EXPRESS graphical user interface. Logically related options are grouped in common panels as described in the text.

Table 1
EXPRESS simulation options. Listed with each option is the relevant time scale (kinetic window) based on typical values for the relevant interaction strengths. A separate, self-contained subroutine is used to simulate each type of experiment, based on parameters passed to it as a single data structure.

Experiment	Timescale	Comments
^{2}H QE	10^5–10^7 s^{-1}	Its traditional...
^{2}H T1Z	10^8–10^{12} s^{-1}	IR w/QE detection
^{2}H T1Q	10^8–10^{12} s^{-1}	Broad band excitation w/echo detection
^{2}H QCPMG	10^3–10^8 s^{-1}	Multiple QE train
^{2}H OMAS	10^2–10^8 s^{-1}	Variable Angle Spinning w/CQ only
^{2}H OMAS/CSA	10^2–10^8 s^{-1}	Includes CQ and CSA
I = ½ 1-PULSE	10^2–10^4 s^{-1}	Static and OMAS w/CSA
I > 1 Static	10^5–10^8 s^{-1}	Central transition only
I > 1 OMAS	10^5–10^8 s^{-1}	Central transition only
I > 1 QCPMG	10^5–10^8 s^{-1}	Central transition only
(user routine)	—	User-defined experiment

Site-specific parameters needed to define a motional model are entered from the "Site Definitions" panel. An arbitrary number of jump frames can be defined, and for each frame an arbitrary number of sites can be specified. Each site is defined by a set of three Euler angles that rotate the Cartesian XYZ axes of that frame into the *next* frame. Thus for a one-frame problem (e.g., 3-fold hops as a model of methyl rotation), the site angles rotate each orientation of the relevant tensor *PAS* axes into coincidence with crystal-fixed axes, while for a two-frame problem, the first frame site angles rotate each *PAS* orientation into coincidence with the Cartesian *XYZ* axes of an intermediate jump frame, whose possible orientations with respect to crystal-fixed axes are defined by the site angles specified for the *second* frame. Thus if the user defines N_F frames, with N_1 sites in frame 1, N_2 sites in frame 2, etc, the total number of equivalent "one-frame" sites defined with respect to crystal-fixed axes is $N_T = \prod_{j=1}^{N_F} N_j$.

A comment is in order regarding the site angles used in EXPRESS to specify the orientation of the CSA tensor. In simulations for which *only* the CSA tensor is used, this presents no particular problem. However, quadrupole coupling tensors in EXPRESS make use of (standard, universally used) Abragam/Hahn conventions [44,57] with regard to assignment of principal components to molecule-fixed axes, while CSA tensors make use of *different* (standard, though not quite universal [48]) conventions. Hence, if the transformation angles are specified separately for each tensor, it would not be easy to determine the relation between these angles and the relative orientation of the EFG and CSA tensors for each site. EXPRESS avoids this difficulty by the pragmatic expedient of directly specifying the latter whenever possible. Thus, for simulations that make use of both EFG and CSA tensors, the Euler angles specified for each site orientation are those for the EFG tensor, while those specified for the CSA tensor in that site rotate the principal CSA axes into coincidence with those of the EFG tensor. Thus, by setting α_{CSA}, β_{CSA}, and γ_{CSA} equal to zero for a given site implies coincidence of the CSA and EFG tensor axes for that site unless the EFG tensor is zero, in which case Ω_{CSA} specifies the orientation of principal CSA components directly.

Unlike its ancestors MXQET [23] and MXET1 [26], EXPRESS follows the standard [39] convention that (ultimately) expresses the possible orientations of a crystal-fixed reference frame with respect to principal Cartesian axes of the relevant interaction tensor. However, it is much easier to visualize the motion with respect to crystal-fixed axes. This requires specifying the rotational jumps in terms of the *inverse* rotation, e.g., the three possible orientations of

a C–D bond in a methyl group that executes 3-fold hops. To help ensure that user-entered site angles describe the intended rotation, EXPRESS features a "view sites" option that, for each frame, displays a color coded animation of three Cartesian axes hopping between orientations defined by rotations inverse to those entered by the user. In addition, the complete set of N_T one-frame equivalent Euler angles that rotate each specified orientation directly from the *PAS* to the crystal-fixed reference frame are computed and displayed.

As mentioned in the preceding section, it is often sufficient to define rotational jumps from site to site within a given frame in terms of a single rate constant. This is the default option in EXPRESS, together with a limited menu of site "connectivities" that includes all sites (jumps with equal probability from each site to any other), jumps along a chain ($k_{i,i+1} = \delta_{i,i+1}$), and jumps around a ring ($k_{i,i+1} = \delta_{i,i+1}$ and $k_{1,Nj} = 1$). It is also possible to display and edit each frame-specific rate matrix K_F, to define jumps at any desired rate between any pair of sites in that frame. Then, EXPRESS automatically builds the equivalent one-frame rate matrix using the templates and jump rates defined for each frame. Implicit in this procedure is the requirement that the rates and site connectivity defined in any given frame are independent of those in any other frame. This could be a serious limitation in practice: for example, in the interior of a hydrophobic protein the barrier to side chain methyl rotation could be strongly dependent on the orientation of the methyl spinning axis relative to nearby bulky groups. To allow for this and other kinds of correlated jump processes, EXPRESS offers the option of graphically displaying and editing the entire one-frame rate matrix element by element.

After specifying frames, site orientations and rates, it remains to complete the simulation model by specifying site-specific parameters that can are best defined directly in the one-frame representation. These include principal tensor components (the default is equal tensor components in all sites) and the relative weights or site populations.

3.1. Unequal site populations

All of the frame-specific rate matrix templates (and the resulting one-frame rate matrix) are maintained internally as symmetric matrices, with diagonal elements automatically computed initially as negative sums of off-diagonal elements in the corresponding rows (or columns). However, if two sites have unequal populations p_j and p_k, the one-frame K-matrix must be modified to satisfy the principle of microscopic reversibility, $p_j k_{kj} = p_k k_{jk}$, where k_{jk} is defined as the rate of jumps *from* site k *to* site j. (We note in passing that this convention is transposed from that used in many discussions of stochastic processes, but is entirely consistent with early discussions of N-site chemical exchange [58]).

In order to avoid numerical difficulties associated with asymmetric matrices, EXPRESS makes use of a well-known mathematical procedure for symmetrizing the matrix representation of the Liouvillian operator. For example, Eq. (2) applied to the case of free precession of an exchange-coupled set of N single quantum coherences yields the expression

$$S(t) = 1 \cdot e^{At} \cdot \mathrm{w} \tag{20}$$

where $S(t)$ is the free induction decay signal, A is the asymmetric matrix $(i\Omega + K)$, 1 stands for the unit vector, and w is a column vector of site populations. Defining a diagonal matrix whose elements are $P_{jk} = \delta_{jk} p_j^{1/2}$, Eq. (20) transforms to the symmetric form

$$S(t) = w^{1/2} \cdot e^{\tilde{A}t} \cdot w^{1/2} \tag{21}$$

where $\tilde{A}$ is given by

$$\tilde{A}_{jk} = [P^{-1} A P]_{jk} = i\Omega_j \delta_{jk} + \tilde{K}_{jk} \tag{22}$$

with

$$\begin{aligned} \tilde{K}_{jk} &= k_{jk} (p_k / p_j)^{1/2} \\ \tilde{K}_{kj} &= k_{kj} (p_j / p_k)^{1/2} = \tilde{K}_{jk} \end{aligned} \tag{23}$$

The EXPRESS simulation routines all make use of this symmetrizing procedure, and never directly compute matrix functions of asymmetric matrices. However, unpleasant numerical instabilities can still arise if the "jump rate" entered by the user is taken to be k_{jk} as defined in Eqs. (21)–(23) and the population p_j is allowed to become small. To avoid such problems, jump rates entered in the EXPRESS rate matrix templates are always interpreted as the *arithmetic mean* of the forward and reverse rates, $k = (k_{jk} + k_{kj})/2$. This implies that off-diagonal elements $\tilde{K}_{jk}$ are given by the numerically stable relation

$$\tilde{K}_{jk} = \tilde{K}_{kj} \frac{2k (p_j p_k)^{1/2}}{p_j + p_k} \tag{24}$$

It can be shown that while the *diagonal* matrix element $\tilde{K}_{jj} = K_{jj} = -\sum_{k \neq j}^{N} k_{jk}$ is still just minus the inverse lifetime in site j, the definition of k as the arithmetic mean of forward and reverse rates has the somewhat disconcerting consequence that $-\tilde{K}_{jj}$ is *not* equal to the sum of off-diagonal elements in the corresponding column of $\tilde{K}$.

3.2. Algorithms and computational efficiency

EXPRESS simulates time domain signals for each of the experiments listed in Table 1 by evaluating a (non-unitary) matrix propagator $E(\Delta t)$ where Δt is the user-specified dwell time, and then computing the N values of the vector M of relevant single quantum coherences by recursion relations of the form

$$M_{n+1} = M((n+1)\Delta t) = E \cdot M_n \tag{25}$$

Eq. (25) (and the evaluation of the propagator itself) is carried out inside a loop over a user-defined set of powder increments.

For non-rotating samples, the key step in computing the propagator is evaluation of the matrix exponential, $\exp(A\Delta t)$, where A is the complex, non-Hermitian matrix given in Eq. (2). EXPRESS accomplishes this time consuming task using the built-in MATLAB routine EXPM. Timing tests reveal that this procedure is typically more efficient than direct diagonalization of A itself, perhaps because the latter procedure requires computing both left and right eigenvectors. MATLAB matrix routines make use of precompiled, platform-specific optimized libraries for matrix operations, and are significantly more efficient than FORTRAN routines previously used, for example, in MXQET. Times required for typical simulations of experiments on non-rotating samples are summarized in Table 2 and for rotating samples in Table 3.

Table 2
Representative simulation times for experiments on non-rotating samples.

Experiment	Sites[a]	Points	Tiles[b]	Other	CPU time[c] (s)
2H QE	3 × 4	512	233	—	3.1
2H QE	3 × 7	512	233	—	4.2
2H QE	3 × 7	512	1597	—	28.2
2H QE	10 × 3	256	987	—	17.5
2H QE	20 × 3	256	987	—	74.4
2H T1Z	3 × 4	512	233	8 τ-values	16.3
2H T1Q	3 × 4	512	233	8 τ-values	17.7
2H QCPMG	3 × 4	8192	233	136 echoes	30.4
$I > 1$ Static	4	256	987	CQ + CSA	6.9

[a] $n \times m$ stands for a simulation with m sites in frame 1 and m sites in frame 2.
[b] Tiles is the number of (α, β) pairs chosen by the ZCW algorithm.
[c] Simulation times for a 2 GHz PowerMac G5 running MATLAB release r2007b under Mac OSX 10.5.

Table 3
Representative simulation times for experiments on rotating samples.

Experiment	Sites[a]	υ_R[b]	Pairs[c]	Size[d]	Points	Tiles[e]	CPU time[f] (s)
2H OMAS	3×4	25	4	108	256	144	18.8
2H OMAS/CSA	3×4	25	4	108	256	144	39.8
2H OMAS	3×4	25	4	108	512	144	22.1
2H OMAS	3×7	25	4	189	256	144	95
2H OMAS	3×7	25	4	189	512	144	116
2H OMAS	3×7	25	4	189	1024	144	209
2H OMAS	3×7	25	4	189	2048	144	323
2H OMAS	3×7	25	6	273	2048	144	737
2H OMAS	3×17	6	15	144	8192	144	62208
$I > 1$ OMAS	3×4	35	3	84	256	987	86

[a] $n \times m$ stands for a simulation with m sites in frame 1 and m sites in frame 2.
[b] Spin rate (kHz).
[c] Number of sideband pairs, user-selected to be ~2–3 times the number of observable pairs.
[d] Floquet matrix size.
[e] Tiles is the number of (α, β) pairs chosen by the ZCW algorithm.
[f] Simulation times for a 2 GHz PowerMac G5 running MATLAB release r2007b under Mac OSX 10.5.

It is evident from the timing comparisons in Tables 2 and 3 that the time required for an EXPRESS simulation varies from a few seconds to several minutes or more depending on the particular experiment and the number of sites, powder tiling increments, and FID points computed. For models with up to 20–30 sites, it is often possible to compute an adequately accurate line shape (or set of partially relaxed line shapes) in less than a minute or two. The simulation time is *not* a strong function of site connectivity, the relative magnitudes of site frequency differences and jump rates, or the nature of the tensor interactions. Wide powder patterns require far more time to simulate than narrow ones, since more powder increments are then needed to achieve convergence.

MAS simulations tend to be more time consuming than corresponding simulations for non-rotating samples, because simple matrix exponentiation fails when the site frequencies are time dependent. Within the framework of discrete site-to-site jumps, it is possible by means of Floquet theory to replace $A(t)$ by a much larger, but time *independent* matrix A_F [29,50,59]. The line shape, including MAS and OMAS sidebands, can then be computed by a formalism identical to that used for non-rotating samples. Levitt et al. [12,60] compared the efficiency of the Floquet approach to computation of the matrix propagator by subdividing the rotor period into a sequence of short intervals Δt for which $A(\Delta t)$ is effectively time independent. They concluded that this direct approach is usually more efficient [12], especially for a large number of sites. However, advances in computer power and the technology of MAS NMR prompted us to re-examine this conclusion. In particular, MAS probes that spin at rates up to 65–70 kHz are now commercially available, and special purpose probes capable of spinning at rates up to 80 kHz have been described in the literature. For these fast spin rates, the number of spinning side bands (and hence the number of required Floquet states) is not prohibitively large, even for a full width deuteron powder spectrum. Moreover, code profiling reveals that even for large scale MAS simulations (matrix size ~1000), as much as 80% of the CPU time used by EXPRESS is spent on recursive FID propagation rather than matrix exponentiation. Perhaps this is a consequence of MATLAB's internal use of Pade approximants rather than full eigenvalue calculations for matrix exponentials. In any case, the Floquet approach used in EXPRESS is adequate for all but the most time consuming simulations. (The largest simulation we have done is a 57-site ^{2}H MAS simulation with 233 powder increments, 8192 FID points, and 12 sideband pairs (matrix size 1425×1425) that required ~9 h of computer time on a 2.3 GHz dual-processor Mac Powerbook Pro, running 64 bit MATLAB).

3.3. Parameter optimization

For a general N-site jump problem with quadrupole coupling and chemical shift anisotropy there are, in principle, $13N - 1 + N(N-1)/2$ independent parameters: $2N$ principal EFG tensor components, $3N$ principal CSA tensor components, $6N$ independent sets of *PAS* tensor orientations, $N - 1$ relative populations, and $N(N-1)/2$ independent jump rates. Thus for a 20 site problem, EXPRESS requires specification of no less than 437 parameters. The situation is somewhat analogous to classical molecular dynamics (MD) simulations of the trajectories of N interacting particles: in neither case is it possible or appropriate to "determine" all the relevant parameters by matching simulations to the results of any particular experiment. For N-site jump problems in solid state NMR, a crucial part of defining the model is inventing a procedure to reduce the number of adjustable parameters to a tractable value such as three or four.

In many cases, it is possible to estimate values of the principal tensor components by theoretical computation or measurements on related materials, and to reduce the number of site orientations by invoking local symmetry. However, the number of adjustable parameters is still uncomfortably large, especially for models of small angle motion along a multi-dimensional angular trajectory. An excellent example of one way to proceed in this commonly occurring situation has recently been described by Meints et al. [61], who used the procedure of Nadler and Shulten [62] to make a discrete, tri-diagonal approximation to the Smoluchkowski operator for rotational diffusion subject to a multi-dimensional potential energy function. A different option, perhaps more appropriate for disordered systems, is described in Section 4.

EXPRESS preserves all the parameters needed for a simulation in a single data structure, which is saved on disk and passed as an argument to individual subroutines specific for particular experiments. It is therefore straightforward, in principle, to incorporate those subroutines in automatic fitting programs designed to deliver best fit parameter values by nonlinear least squares procedures. In practice this approach is rather inefficient (each iteration on a set of N parameters requires at least $2N$ complete simulations for gradient-based algorithms). It would also be advisable to incorporate user-defined constraints, such as positive jump rates. A better use of the EXPRESS simulation routines is to incorporate the parameter file and calls to the simulation routine in a MATLAB script that generates libraries of simulations in which relevant parameters are stepped through user-defined ranges. Constructing such a library may take hours or even days of computation time but once built, the library can be used as a look-up table for very efficient identification of minima in least squares error surfaces.

Matching EXPRESS simulations to experimental relaxation time data presents special problems. It is definitely not a good idea to try to match EXPRESS simulations to a set of experimentally partially relaxed line shapes: the latter are subject to artifacts associated with finite pulse width effects while EXPRESS assumes artifact-free, δ-function pulses. The most important finite pulse artifact is that of non-uniform initial excitation, which leads to significant distortion of the partially relaxed line shape at intermediate values of the recovery delay time. In addition to a (minimal) set of standard routines for data processing (left shifts, apodization, Fourier transformation, phase correction, etc), EXPRESS includes a set of utilities for fitting a three-parameter, single exponential recovery function to user-defined points in a simulated set of partially relaxed line shapes. Even in cases where the simulated (and experimental) recovery curves are mildly non-exponential, matching these simulated "anisotropy profiles" to those generated by the same procedure applied to real experimental data avoids most of the pitfalls associated with finite pulses.

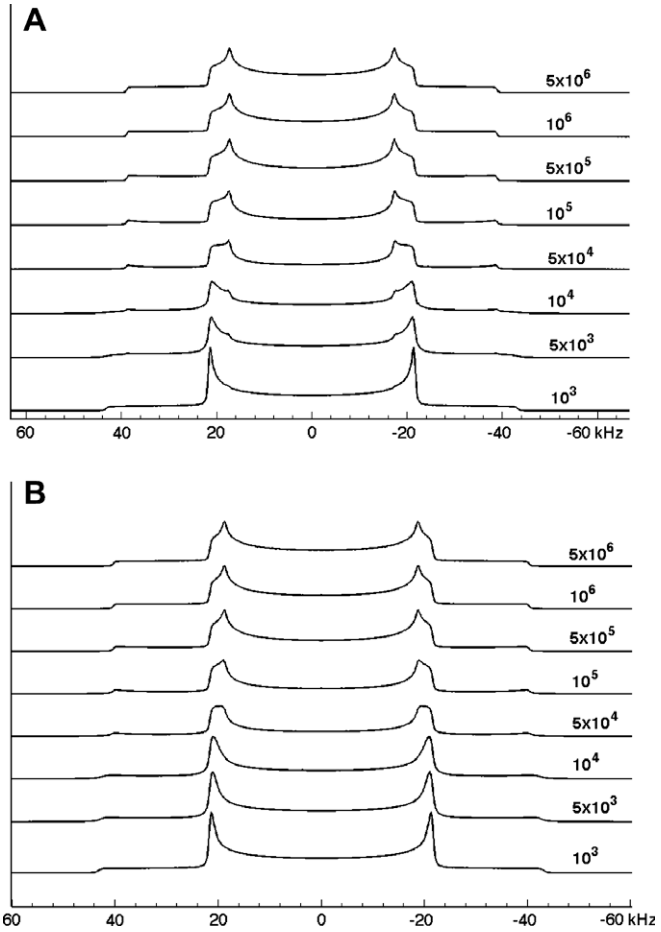

Fig. 2. Simulated quadrupole echo spectra for a librating, rotating methyl group. (A) Libration of the methyl spinning axis between two sites along an arc from 0° to 30°. (B) Nearest neighbor jumps among three sites 0°, 15°, 30° along the same arc. Libration rates are indicated next to each line shape, other simulation parameters are given in the text. Note the difference in powder pattern "horn" line shapes for two and three site jumps at intermediate libration rates $\sim 10^5\ s^{-1}$.

4. Illustrative simulations

4.1. ^2H quadrupole echoes

Fig. 2 shows simulated ^2H quadrupole echo spectra for a rapidly rotating methyl group whose rotation axis jumps at rate k_2 between two orientations, $(\alpha_2,\beta_2,\gamma_2)$ = (0,0,0) and (0,30,0) (Fig. 2A) or three orientations, $(\alpha_2,\beta_2,\gamma_2)$ = (0,0,0), (0,15,0) and (0,30,0). In these simulations methyl rotation was modeled as 3-fold jumps at rate $k_3 = 5 \times 10^9\ s^{-1}$, the angle β_1 with respect to the 3-fold methyl rotation axis was 74°, and in all sites the *PAS* values C_Q = 155 kHz and $\eta = 0$ were used.

For both models, fast rotation of the methyl group results in an average quadrupole coupling tensor with $\eta = 0$ and $\langle C_Q \rangle = \frac{1}{2}(3\cos^2\beta_1)C_Q = -59.8$ kHz, whose principal z-axis is coincident with the methyl spinning axis. Librational motion of this axis, when modeled as jumps between different values of Euler angle β_2, reduces the average values of field gradients q_{ZZ} and q_{XX} while leaving q_{yy} unchanged. Thus for fast libration ($k_2 > 5 \times 10^5\ s^{-1}$), both models produce slight further reduction in the average C_Q value and also induce an effective asymmetry parameter whose magnitude depends on the amplitude of the libration. In the intermediate regime, $10^3 < k_2 < 10^5\ s^{-1}$, the line shape near the horns of the powder pattern is sensitive to details of the libration trajectory: two-site jumps between 0 and 30° (Fig. 2A) produce a quite different line shape than 3-site jumps over the same trajectory (Fig. 2B).

4.2. ^2H T_{1Z} simulations

Mechanistic details of motion that is fast enough to completely average site-specific deuteron quadrupole coupling tensors can be investigated by measuring the orientation dependence of spin lattice relaxation times [63,25]. Using an algorithm described originally by Wittebort et al. [24], EXPRESS simulates deuteron spin response to the well known inversion recovery pulse sequence, $180\text{-}\tau_d\text{-}90_X\text{-}\tau_1\text{-}90_Y\text{-}\tau_2$-ACQ, by generating sets of partially relaxed quadrupole echo spectra as a function of the relaxation delay, τ_d. A typical example is shown in Fig. 3.

These spectra were generated for the six-site model whose parameters are listed in Table 4. This is an accurate model for the well known two-site jump motion in dimethylsulfone [64,11,65], augmented with explicit methyl rotation to account for spin lattice relaxation. Note that it is easy to specify the Euler angles that define 3-fold hops in frame 1 (methyl rotation) and the 2-fold motion (π-flips) of the C_3 spinning axis in frame 2. EXPRESS automatically generates and displays the Euler angles

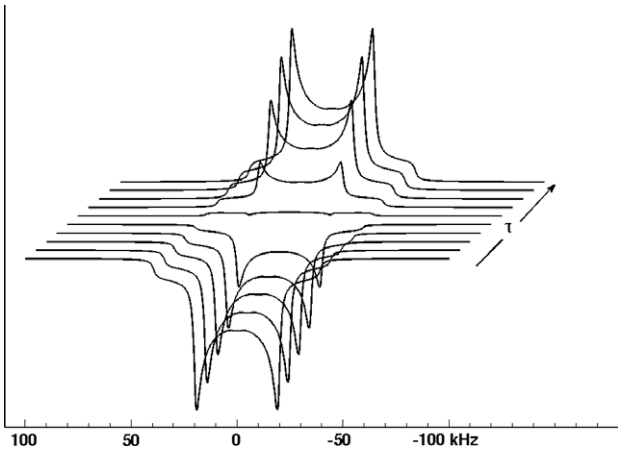

Fig. 3. Partially relaxed ^2H quadrupole spectra simulated in response to an inversion recovery pulse sequence, using parameters given in Table 4.

Table 4
Site angles, jump rates and other parameters for a 2-frame model of librational motion in dimethylsulfone. Motion in frame 1 (rate k_3) is 3-fold hops about the methyl C_{3v} symmetry axis, which itself executes 2-fold π-flips about an axis oriented at 53° to the z-axis of frame 2.

Two-frame parameters					One-frame equivalent sites		
Frame 1 (*PAS*)		α	β	γ	α	β	γ
k_3 $5.0 \times 10^9\ s^{-1}$	1	0	71	0	0	124	0
	2	0	71	120	57.594	55.006	91.714
	3	0	71	240	302.406	55.006	268.206
Frame 2		α	β	γ	0	124	180
k_2 $2000\ s^{-1}$	1	0	53	0	57.594	55.006	271.714
	2	0	53	180	302.406	55.006	88.286

Other parameters	One-frame rate matrix					
C_Q = 160 kHz, $\eta = 0$ (all sites) τ_d		k_3	k_3	k_2		
1,10,20,30,50,100,20,400 ms powder increments	k_3		k_3		k_2	
6765 ZCW echo pulse spacing 30 μs 256 fid points,	k_3	k_3				k_2
no apodization	k_2				k_3	k_3
		k_2		k_3		k_3
			k_2	k_3	k_3	

for an equivalent set of six sites, which are much harder to visualize.

The simulated partially relaxed line shapes should not be matched to experimental spectra, which inevitably suffer distortions (especially near the "null" value (50 ms in Fig. 3) due to imperfect inversion and spectral coverage. Instead, EXPRESS allows the user to define an appropriate window and range of points, and automatically fits the selected points from each partially relaxed spectrum to a three-parameter, single exponential function of the form

$$M(\tau) = M(\infty) + M(0)e^{-\tau_d/T_{1Z}} \tag{26}$$

where $M(0)$ is the initial inversion intensity and $M(\infty)$ is the equilibrium intensity after full recovery. Allowing both these parameters to vary across the line shape (as well as T_{1Z} itself) yields reliable best-fit T_{1Z} values even when inversion is not ideal [26,28]. EXPRESS includes facilities for displaying the resulting best-fit T_{1Z} values as a T_{1Z} anisotropy profile, i.e., a plot of T_{1Z} *vs.* displacement from the center of the line shape. We emphasize that T_{1Z} as defined in Eq. (7) applies only to the total Zeeman magnetization (i.e., the sum of the intensities of each component of the quadrupolar doublet) for a given crystallite, and even in this case the recovery can be non-exponential since many crystallites contribute to the total intensity of a given point on the line shape [63]. Thus, the orientation-dependent relaxation rate determined by fitting each point on the line shape to Eq. (26) represents an operational average. This limitation is, however, not serious. EXPRESS simulations for a wide class of models (including that of Table 4) show that non-exponential recovery only becomes evident after two or three full decades of recovery, and thus very hard to detect. As long as the orientation-dependent relaxation rates are extracted from experimental and simulated spectra obtained by the same procedure over the same range of τ-values, they can be used to determine best fit parameters of motional models. EXPRESS computes T_{1Z} values determined from the recovery of mirror-image points with respect to the center of the line shape.

It is often remarked that motions much slower than the Larmor frequency are too slow to influence spin lattice relaxation, but the situation is more complicated for motions occurring simultaneously on widely different time scales. Fig. 4 compares T_{1Z} anisotropy profiles for fast methyl rotation with those simulated for several values of the two-site jump rate k_2 according to the model in Table 4. The general effect of k_2 is to decrease T_{1Z} near the horns of the powder pattern (~±20 kHz) and increase it at the shoulders (~±20 kHz), thereby decreasing the overall anisotropy. This effect has nothing to do with spin diffusion (a phenomenon that is *not* included in EXPRESS. Within a given crystallite, EXPRESS assigns the same, orientation-dependent T_{1Z} value to all sites, as given by Eq. (7). However, as k_2 increases, it becomes comparable to or larger than the site frequency differences in a progressively larger fraction of crystallite orientations, and any given precession frequency therefore reflects a wider range of crystallite orientations. For the case at hand, this T_{1Z} averaging effect is complete for k_2 >50,000 s^{-1}. EXPRESS will not reproduce the methyl-only anisotropy curve as k_2 tends to zero, because Eq. (7) is not valid in that limit. It is interesting that for this particular model, contributions of the slow process to T_{1Z} are greatest at the shoulders, vanish at the center, and *decrease* with increasing k_2 near the horns of the powder pattern. Whether or not this behavior is model-dependent remains to be investigated.

4.3. ^2H T_{1Q} simulations

For fast and intermediate time scale motion, the anisotropy of T_{1Z} is governed by the underlying anisotropies of the two spectral densities $J_1(\omega_0)$ and $J_2(2\omega_0)$. In absence of ultraslow motion, the decay rate of quadrupole order, $1/T_{1Q}$, is determined by $J_1(\omega_0)$ alone and hence provides complementary information to T_{1Z} [38]. In order to suppress potential complications from magnetization transfer effects (and to increase signal/noise) it is usual to perform such experiments [66] by following the orientation-dependent decay of partially relaxed spectra following more or less uniform, broad band excitation of quadrupole order. EXPRESS includes options for generating and analyzing such spectra. Fig. 5 shows a typical simulated T_{1Q} experiment, with the same parameters used to generate the T_{1Z} experiment in Fig. 3 (except k_2 = 50,000 s^{-1}). In principle, both the $\Delta m = +1$ and $\Delta m = -1$ transitions contribute to the decay of each point inside the horns of the powder pattern.

After ideal, broadband excitation of quadrupole order either the +1 or −1 transition has been inverted (for all crystallite orientations), and according to Eq. (4) will recover as a sum of two exponentials. Only the *difference* between the two transitions decays with time constant T_{1Q}. EXPRESS avoids the 2-fold expense of computing the time evolution of both transitions by a simple trick:

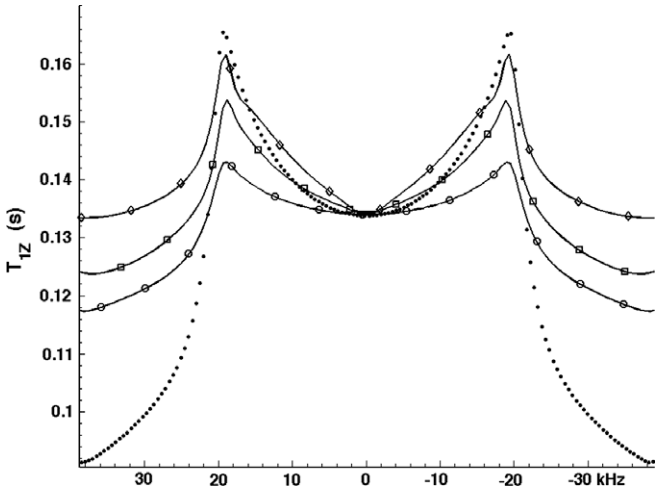

Fig. 4. Simulated T_{1Z} anisotropy profiles for the model defined in Table 4. Circles; k_2 = 2000 s^{-1}. Squares; k_2 = 20,000 s^{-1}. Diamonds; k_2 = 50,000 s^{-1}. Dotted line: anisotropy profile for 3-fold methyl jumps.

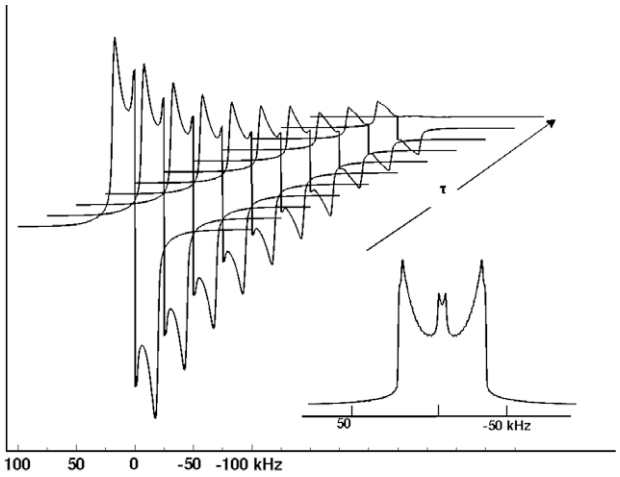

Fig. 5. Stack plot of partially relaxed spectra following initial broad band excitation of quadrupole order, using parameters listed in Table 4 except k_2 = 50,000 s^{-1}. Relaxation delays, τ, between 1 and 400 ms are shown. Inset: equilibrium quadrupole echo spectrum showing a central feature due to intermediate two-site exchange.

Only the $\Delta m = +1$ transition is considered, and signal from each crystallite is assumed to decay exponentially with time constant T_{1Q} given by Eq. (5). After performing the powder average, the frequency domain signal is processed as part of the Fourier transform to ensure that one side of the spectrum is inverted. Clearly, this procedure depends on the assumption of ideal, broadband excitation, and direct comparison of simulated line shapes with experimental ones is not appropriate. Nevertheless, reliable, orientation-dependent values of an effective T_{1Q} can usually be obtained by monitoring the decay of the difference intensity between points symmetrically placed with respect to the center of the powder pattern. (An exception arises if chemical shift anisotropy is large enough to destroy the mirror image powder pattern symmetry). Fig. 6 shows T_{1Q} anisotropy profiles generated in this fashion for the same system considered in Fig. 4.

Even though the computed T_{1Q} values depend only on $J_1(\omega_0)$ and inequality $k_2 \ll \omega_0$ is well satisfied, the slow motion produces the same sort of leveling effect on T_{1Q} anisotropy as it does for T_{1Z}. However, the behavior near the center of the powder pattern is more complicated. For methyl rotation alone (dashed line) T_{1Q} is a maximum at the center of the powder pattern, while for all the simulations with finite k_2 it is actually a minimum. Presumably, this reflects the range of crystallites that contribute to the central feature of the powder pattern as shown in the inset of Fig. 5. While there is experimental evidence (see Fig. 6 of Ref. [65]) that such a minimum exists for dimethylsulfone-d_6 at 298 K, uniform excitation of quadrupole order is especially difficult to create near the center of the powder pattern.

4.4. ^{2}H QCPMG and MAS simulations

Magic angle spinning [11,29] and quadrupolar Carr–Purcell–Meiboom–Gill [30,67] experiments offer similar advantages of signal to noise enhancement with respect to simple quadrupole echo spectra: in both cases, the sensitivity improvement is given approximately by the ratio of the powder pattern line width to the width of a single side band, divided by the number of side bands. Experimentally, enhancements on the order of 20 to 30 are common. This useful feature of the two experiments was a primary motivation for developing algorithms for their simulation. Here, we use EXPRESS to assess the dynamic information accessible from these experiments.

We consider the familiar double-axis rotations that occur in urea [68] and urea inclusion compounds [69,70,15]. The EXPRESS

Table 5
Site angles, jump rates and other parameters for a 2-frame model of double axis π-flips in urea-d_4. Motion in frame 1 (rate k_3) is 180° jumps about the bisector of the D–N–D bond angle, and in frame 2 it is whole-body 180° jumps about the C–O bond axis. Interaction strengths and rates are appropriate [15] for urea-d_4 in an inclusion compound with octanoic acid. For the QE simulation, 256 fid points were computed while for MAS and QCPMG, 4096 points were needed. Fifteen side band pairs were included in the MAS simulation.

Two-frame parameters					One-frame equivalent sites		
Frame 1 (CN)		α	β	γ	α	β	γ
k_{CN} 260 s^{-1}	1	0	58	0	0	175	0
	2	0	58	180	180	59	0
Frame 2 (CO)		α	β	γ	0	175	180
k_{CO} 5 × 10^6 s^{-1}	1	0	117	0	180	59	180
	2	0	117	180			

Other parameters	Onẽ-frame rate matrix			
C_Q = 208 kHz, η = 0 (all sites), QE: 2τ = 40 μs, 46,368 tiles, QCPMG 2τ = 40 μs, 1597 tiles, MAS spin rate 25 kHz 377 tiles		k_{CN}	k_{CO}	
	k_{CN}			k_{CO}
	k_{CO}			k_{CN}
		k_{CO}	k_{CN}	

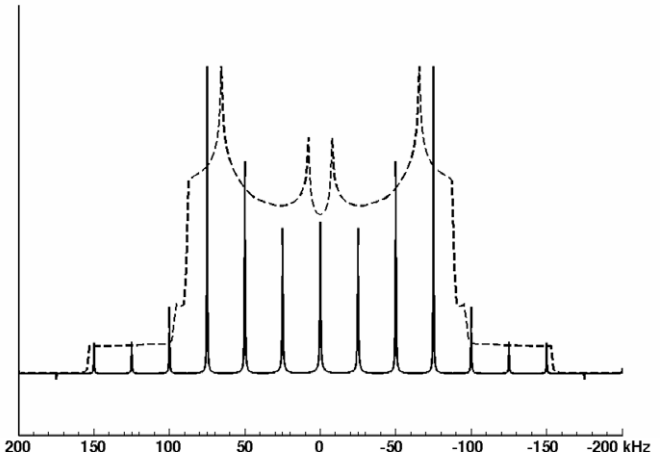

Fig. 7. Simulated QCPMG spectrum (solid line) and quadrupole echo spectrum (dashed line) for urea-d_4 octanoic acid inclusion compound, using parameters listed in Table 5. The quadrupole echo simulation required 244 s cpu time for 256 points with 46,368 tiles, running under 64-bit MATLAB (release R2008b beta) on a 2.3 GHz Macbook Pro. The 4096 point, 377-tile QCPMG spectrum required 159 s.

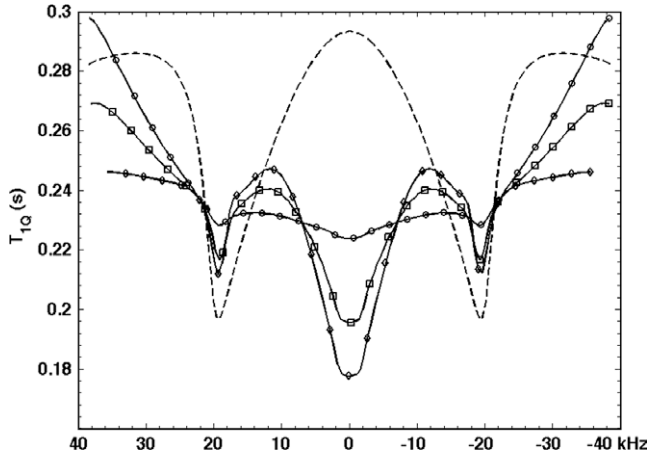

Fig. 6. Simulated T_{1Q} anisotropy profiles for the model defined in Table 4. Circles; k_2 = 2000 s^{-1}. Squares; k_2 = 20,000 s^{-1}. Diamonds; k_2 = 50,000 s^{-1}. Dashed line: anisotropy profile for 3-fold methyl jumps.

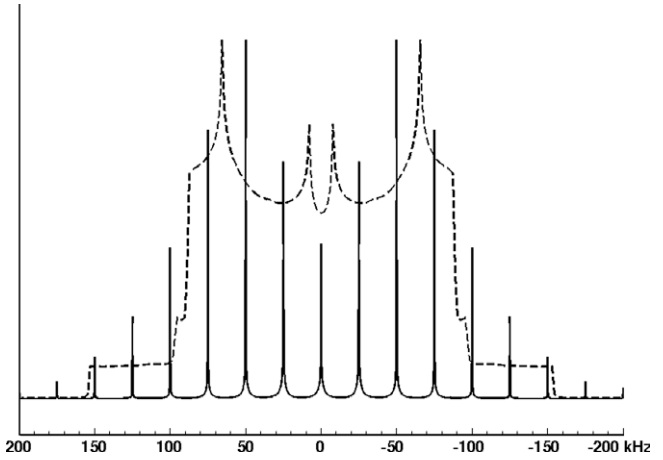

Fig. 8. Simulated MAS spectrum (solid line) and quadrupole echo spectrum (dashed line) for urea-d_4 octanoic acid inclusion compound, using parameters listed in Table 5. The 4096 point, 1597-tile MAS simulation required 121 s cpu time, running under 64-bit MATLAB (release R2008b beta) on a 2.3 GHz Macbook Pro.

parameters summarized in Table 5 for this system are those obtained by fitting ^{2}H OMAS data obtained at 46 MHz and 333 K [15]. Note that the site order and angles differ from those reported in Ref. [15], in which Euler angle β refers to rotation about the intermediate x rather than y-axis. Also, due to a misunderstanding about the philosophical meaning of π, the rotor offset angles reported in Ref. [15] are about three times smaller than those actually used. The simulated QCPMG (Fig. 7) and MAS (Fig. 8) spectra both consist of narrow side bands, whose intensity envelope approximates the profile of the quadrupole echo spectrum (dashed line).

The rapidly decaying quadrupole echo signal required computation of only 256 points (dwell time 2.5 μs), but this is more than offset by the need to compute no less than 46368 ZCW tiles to achieve convergence to a smooth powder line shape. Even though the narrower lines of the MAS and QCPMG spectra required computation of 8 times more points, these simulations were complete in ~1/2 to 2/3 the time of the QE simulation. This is a manifestation of the same phenomenon that gives better signal to noise ratio for MAS and QCPMG experiments: concentration of the observed signal into narrow spectral regions. As expected, simulations for off-magic angle spinning (data not shown) require more powder increments and become rapidly more time consuming as the rotor angle deviates from the exact magic angle condition.

For both MAS and QCPMG, the envelope of sideband intensities is sensitive to roughly the same kinetic window as the QE spectrum and the side band line widths extend both ends of the kinetic window by about an order of magnitude. However, the mechanism of echo formation is entirely different in the two experiments. This leads to a subtle difference in the side band line widths, as demonstrated in Fig. 9.

In the MAS simulation, side band line widths are almost constant while for QCPMG, side bands outside the powder pattern horns are ~2.5 times sharper than in the middle of the spectrum. This phenomenon can be understood qualitatively by considering the MAS experiment in terms of a time *independent* reference set of crystallites defined by a common, fixed orientation of the rotor axis in the crystal-fixed frame [71]. Sample rotation carries individual crystallites into and out of this frame, typically at a rate fast enough compared with the difference in their orientation-dependent transverse relaxation rates to result in significant averaging. No such transport occurs for a stationary sample, and the line widths for different side bands therefore reflect contributions from different sets of crystallite orientations.

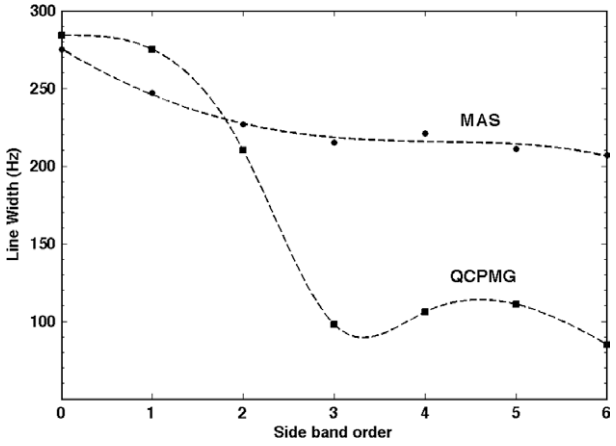

Fig. 9. Side band line widths determined from the QCPMG and MAS simulations shown in Figs. 7 and 8, respectively. Dashed lines connecting the points are meant only to guide the eye.

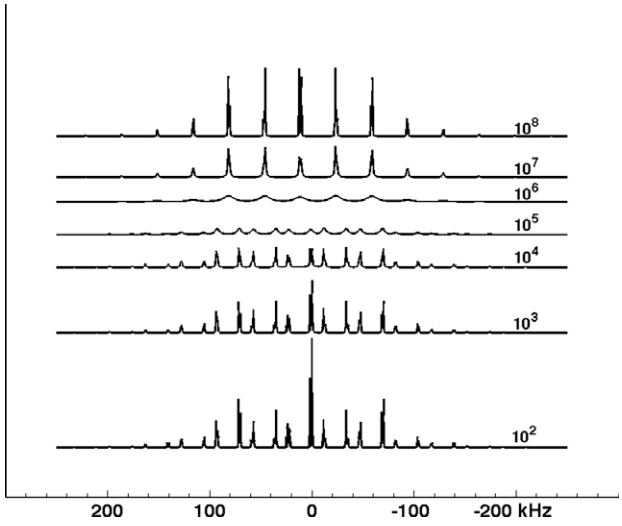

Fig. 10. ^{2}H OMAS (115.1 MHz) simulation of bulk liquid-surface exchange with one diamagnetic and one paramagnetic surface site. The rotor spinning axis is offset 0.5° from the magic angle. The jump rate is indicated in the figure for each simulation. Other EXPRESS parameters for this model are given in the text.

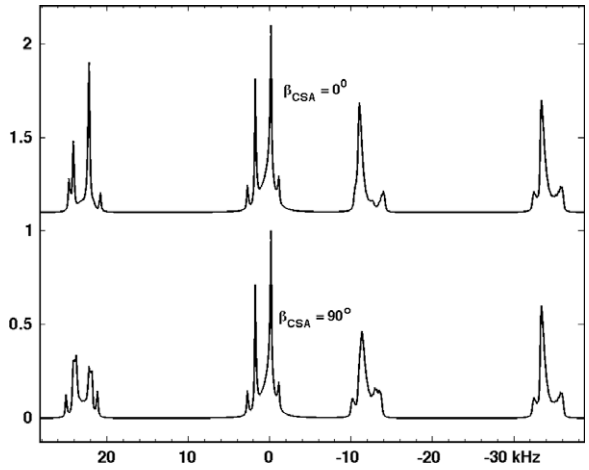

Fig. 11. Bottom trace: Expanded scale of the central region of the spectrum from Fig. 10 for jump rate 100 s^{-1}. Top trace: simulated spectrum with the same parameters except that the paramagnetic tensor for the surface site has coincident principal axes with the electric field gradient tensor.

4.5. ^{2}H dynamics in paramagnetic systems

EXPRESS offers the option of including chemical shift anisotropy simultaneously with first order quadrupole coupling in MAS and OMAS simulations. This is rarely necessary for diamagnetic materials even at high fields, since sample rotation at speeds ~25 kHz or higher is sufficient to suppress all but the largest deuteron chemical shift anisotropy. However, for paramagnetic materials, the large electron-nuclear dipolar coupling combined with g-tensor anisotropy produces an interaction that is formally equivalent to chemical shift anisotropy [72] but quite comparable in magnitude to quadrupole coupling. Figs. 10–12 illustrate several features of EXPRESS that may prove useful for understanding jump dynamics in such systems.

We consider a hypothetical three-site model for an acetylenic deuteron characterized by quadrupole coupling constant C_Q = 200 kHz and asymmetry parameter η = 0. Site 1, chemical shift σ_{iso} = 7 ppm, represents deuterons adsorbed at a diamagnetic site on a catalytic surface. Site 2, representing an isotropic liquid, has zero quadrupole coupling and zero isotropic chemical shift. Site 3

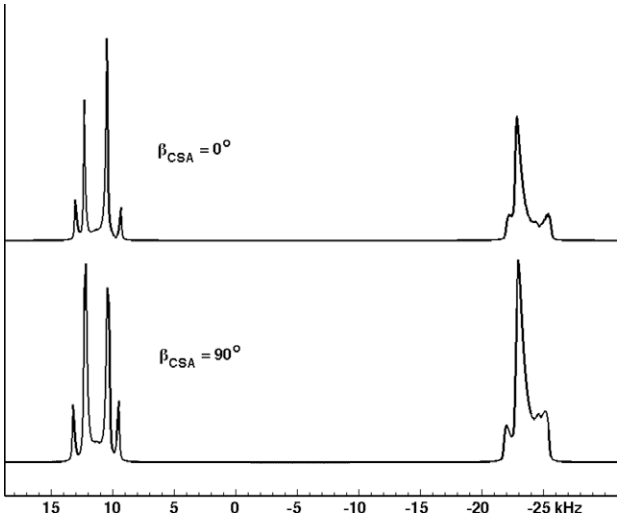

Fig. 12. Bottom trace: expanded scale of the central region of the spectrum from Fig. 10 for jump rate $10^8\ s^{-1}$. Top trace: simulated spectrum with the same parameters except that the paramagnetic tensor for the surface site has coincident principal axes with the electric field gradient tensor.

is a paramagnetic surface site for which the effective CSA tensor has $\Delta\sigma = 500$ ppm, $\sigma_{iso} = 200$ ppm, $\eta = 0.5$, and a principal z-axis rotated by angle β_{CSA} with respect to the principal z-axis of the quadrupole tensor in site 1. Sites 1 and 3 have equal population and cannot exchange directly, but both can exchange at the same rate with liquid site 2, whose population is only 0.1 that of sites 1 or 3. Simulated OMAS spectra (spin rate 35 kHz, OMAS offset 0.5°, Larmor frequency 115.1 MHz) are shown in Fig. 10 for jump rates between 100 and $10^8\ s^{-1}$.

The Floquet basis included 25 states for each site. The simulated free precession signals at either end of the kinetic window needed 8192 simulation points to reproduce the decay of narrow spectral features, and 4181 ZCW tiles for a convergent powder average. Each such simulation required ~1 h of cpu time; much less time was needed for intermediate jump rates.

The low population of site 2 (liquid) causes its spectrum (a single line at zero frequency) to broaden most rapidly with increasing jump rate. Direct exchange between surface sites is not permitted by the model, but the indirect 1–2–3 two step exchange nevertheless broadens the sideband manifolds associated with surface sites 1 and 3 and these begin to collapse as the jump rate approaches 2π (200 ppm × 115 MHz) $\approx 10^5\ s^{-1}$. For faster jump rates, the spectrum sharpens into a manifold of side bands characterized by a single, motionally averaged quadrupole coupling tensor and a single, averaged paramagnetic tensor. The advantage of investigating such phenomena via OMAS rather than exact magic angle spinning arises from the controlled reintroduction of the second rank tensor interactions, manifested in the shape of individual side bands. Some of these are shown on expanded scale in Figs. 11 and 12.

In Fig. 11 (jump rate $100\ s^{-1}$), the multiplet near zero is the center band for (diamagnetic) sites 1 and 2, the feature near −35 kHz is the first spinning side band for site 1 (site 2 has no side bands), and the features near +23 kHz and −12 kHz are the center band and first side band for paramagnetic site 3. The side band fine structure for the diamagnetic site, which arises exclusively from the quadrupole coupling, in characteristically different from that due to the paramagnetic site, which arises from a combination of quadrupole coupling and the paramagnetic coupling tensor. Moreover, the latter depends not only on the relative magnitude of the two tensors but also on their relative orientations. In the fast motion limit, Fig. 12, where the center band and all sidebands are governed by motionally averaged tensors, information about the relative tensor orientation is still apparent.

Compared with the slow motion spectrum, the differences in band shape between $\beta_{CSA} = 0°$ and $\beta_{CSA} = 90°$ are more subtle, because the averaged paramagnetic tensor has been reduced by the exchange process while the quadrupole coupling tensor has not (except for the ~5% decrease in both tensors contributed by residence in the isotropic liquid site).

We emphasize that EXPRESS is an appropriate vehicle primarily for theoretical investigations of various models for jump motion of deuterons in paramagnetic environments. Before using it to match real experimental data, it would be advisable to incorporate additional features for including site-dependent paramagnetic contributions [73] to transverse relaxation rates.

4.6. High spin quadrupolar nuclei

Quadrupolar nuclei with (half integral) spin greater than one comprise nearly three quarters of NMR-active nuclei, but it has only recently become possible to obtain high resolution, solid state NMR spectra. MAS spectra of the central transition is the most widely used technique. There is growing recognition [74,16,17,75] that dynamic information can be obtained from such spectra by methods analogous to those familiar to practitioners of deuteron solid state NMR. EXPRESS was developed, in part, to extend the general formalism for deuterons to nuclei with higher spin. As noted in Table 1, facilities are included for simulating non-spinning powder line shapes, QCPMG multiple echo trains, and MAS/OMAS spectra for spin 3/2, 5/2, 7/2 and 9/2 governed by a combination of second order quadrupole coupling and anisotropic chemical shift interactions. EXPRESS does not include routines for jump-dynamic contributions to spin lattice relaxation of high spin quadrupoles, although such routines would be easy to implement, because in most cases the dominant relaxation mechanism involves spin-phonon coupling rather than single-particle jumps [76,53].

Figs. 13 and 14 illustrate features of dynamic line shapes that appear only for second order quadrupole interactions. We consider a system with three sites, defined by Euler angles $(\alpha,\beta,\gamma) = (0,0,0)$, $(\pi,\pi2,\pi2)$, and $(\pi2,\pi2,0)$. It is easy to verify that the Cartesian electric field gradient tensor in crystal-fixed axes is diagonal in all three sites, with principal components diag(q_{XX}, q_{YY}, q_{ZZ}), diag($-q_{YY}, q_{ZZ}, q_{XX}$), and diag(q_{ZZ}, q_{XX}, q_{YY}), respectively. It follows that in the fast motion limit, all three components of the average electric

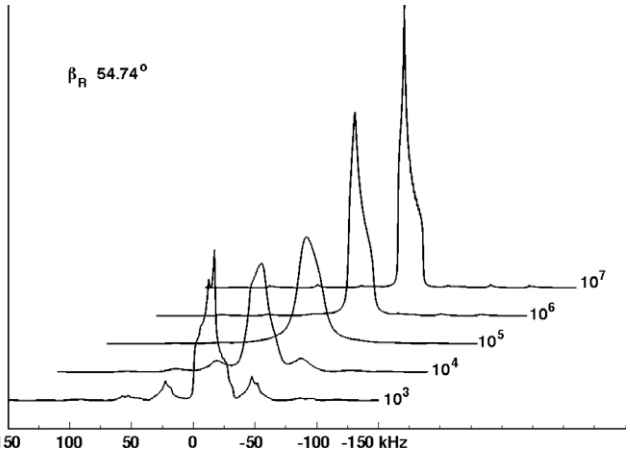

Fig. 13. Simulated 35 kHz MAS spectra ($\beta_R = 54.74°$) for the central transition of 183.3 ^{93}Nb with second order quadrupole coupling, undergoing jumps among three sites such that the motionally averaged quadrupole coupling tensor is zero. The jump rate (s^{-1}) is indicated for each spectrum.

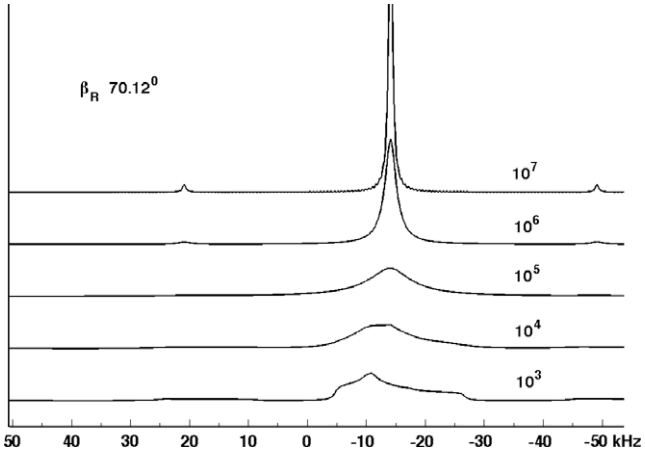

Fig. 14. Simulated 35 kHz OMAS spectra ($\beta_R = 70.12°$) for the central transition of 183.3 ^{93}Nb with second order quadrupole coupling, undergoing jumps among three sites such that the motionally averaged quadrupole coupling tensor is zero. The jump rate (s^{-1}) is indicated for each spectrum.

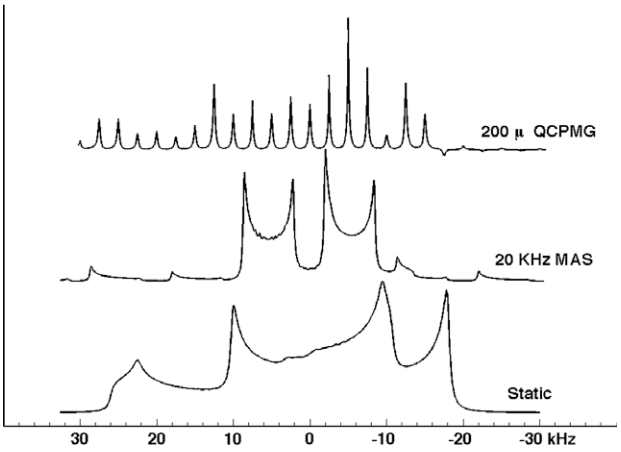

Fig. 15. Simulated central transition line shapes for exchange of a spin 7/2 nucleus between two sites, characterized by different quadrupole coupling and chemical shift tensors. The slow jump rate, 1000 s^{-1}, is responsible for the side band line widths in the QCPMG simulation (upper trace), but has no appreciable effect on either the MAS spectrum (middle trace) or the static line shape (bottom trace). Other simulation parameters are given in Table 6.

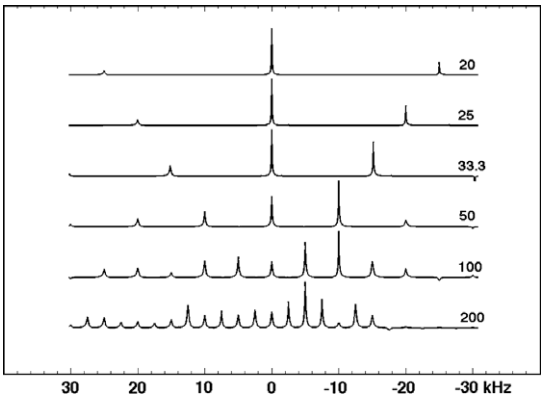

Fig. 16. Simulated QCPMG spectra for the same system as in Fig. 15, with different values of the pulse spacing 2τ (μs). In each spectrum, side bands occur at integer multiples of $1/(2\tau)$. For reasons discussed in the text, side band line widths decrease sharply with decreasing pulse spacing.

field gradient tensor are zero. Fig. 13 shows line shapes simulated as a function of jump rate for a 35 kHz MAS experiment (rotor axis angle $\beta_R = 54.7356°$) on the central transition for a spin 9/2 nucleus with $C_Q = 40$ MHz and $\eta = 0.7$ in all sites. (These are typical parameters for ^{93}Nb in perovskite oxides [77]). As described previously by Schurko et al. [16], model-dependent line shape changes are expected when the jump rate is comparable to the width (in rad/s) of the rigid lattice MAS spectrum, $2\pi(2 \times 10^4) \approx 10^5$ s^{-1} in this example. Fig. 13 also shows, as expected, that jumps occurring on the same time scale as the rotor period interfere with MAS side band formation. Also as noted by Schurko et al. [16], the fast motion limiting line shape is *not* the one computed for a fully averaged quadrupole coupling tensor (zero in the present example), because the site frequencies being averaged are those for a Hamiltonian truncated at second order. The resulting frequencies have tensor components of rank zero (the isotropic second order quadrupole shift), rank 2, and also rank 4. Fast spinning with $\beta_R = 54.7356°$ eliminates the rank 2 contribution, so the center band (and residual side band) line shape in Fig. 13 depends primarily on the rank 4 contributions. These have lower symmetry than the rank 2 contributions and do not average to zero in the fast limit. Also, the orientation-independent rank zero contribution amounts to a (negative) offset of the spectrum that is independent of jump rate since all sites are assumed to have the same quadrupole coupling constant.

Fig. 14 shows line shapes simulated with the same parameters as Fig. 13 except the rotor axis angle is now $\beta_R = 70.1246°$, such that $P_4(\beta_R) = 0$.

In this case the 4th rank contributions are removed by spinning and the resulting line shapes reveal effects of motion on just the second rank terms. As expected, these contributions *do* vanish for jump rates much larger than $\sim 10^5$. However, the averaging is still not complete in the sense that the orientation-independent zero rank term remains. Thus, EXPRESS simulations (and all previously published simulations of second order quadrupole dynamic line shapes) fail to reduce to the proper limit as the jump rate approaches infinity. For jump rates larger than the Larmor frequency ($2\pi \times 183 \times 106 \sim 10^9$ s^{-1} in this example), it is not correct to truncate the Hamiltonian used to construct the stochastic Liouville operator without first diagonalizing contributions from the (dominant) rate matrix. The latter procedure, if done exactly, should be valid for all jump rates. However, this procedure is prohibitively time consuming for all but the simplest problems, since *all* elements of the spin density matrix must be considered for every site. A more effective procedure (at least for non-spinning samples), valid when all the jump rates are on the order of the Larmor frequency or higher, is to first average the *complete* quadrupole Hamiltonian over the motion, expand the result to second order in the usual way, and assign an orientation-dependent width to each powder increment using Redfield theory. We note in passing

Table 6
Simulation parameters for two-site exchange of ^{139}La with second order quadrupole coupling and chemical shift anisotropy.

Experiment[a]	Tiles[b]	Points	cpu time[c] (s)
1-pulse static line shape	28,757	512	252
25 kHz MAS ($\beta_R = 54.74°$)	6765	512	155
QCPMG[d] $\tau = 50$ μs	377	16,384	84
QCPMG $\tau = 200$ μs	610	16,384	136

[a] In both sites, $C_Q = 15$ MHz and $\eta = 0$.The Euler angles for the EFG tensor are (0,0,0) in site 1 and (0,90,0) in site 2. The CSA tensor is zero in site 1 but in site 2, $\delta_{iso} = 100$ ppm, $\Delta\sigma = -200$ ppm, and $\eta_{CSA} = 0.5$. The jump rate is 1000 s^{-1}.

[b] Two-angle ZCW tiling was used for the static and QCPMG simulations, three-angle tiling was used for the MAS simulation.

[c] cpu times refer to a 2.0 GHz PowerPC G5 running MATLAB release R2007b under MAC OSX 10.5.4.

[d] The spectral window for QCPMG simulations was 1000 MHz to ensure sufficient points per echo, and 100 kHz for the other simulations.

that the imaginary part of the Redfield spectral density corresponds to a residual (downfield) frequency shift.

Figs. 15 and 16 illustrate how EXPRESS can be used to investigate the different effects of jump dynamics on static line shapes, MAS line shapes, and QCPMG line shapes for high spin quadrupolar nuclei. The simulations in these figures were all computed for two-site jumps with rate 1000 s^{-1}, for a spin 7/2 nucleus such as ^{139}La that resonates at 105.9 MHz in a 17.6T magnetic field. The quadrupole coupling parameters C_Q = 15 MHz, η = 0 are the same in both sites, but the field gradient is site 2 is rotated 90° (about y) with respect to the site 1 principal z-axis. Also, the chemical shielding tensor is zero in site 1 but in site 2, δ_{iso} = 100 ppm, $\Delta\sigma = -200$ ppm, and η_{CSA} = 0.5. Computational details of the simulations are summarized in Table 6. Even though 19 Floquet states per site were needed to ensure convergence, the MAS simulation required only ~60% as much cpu time as the static line shape, because many fewer tiles were needed. The required number of tiles (both for QCPMG and MAS) decreases rapidly with the number of sidebands that have significant intensity. Thus, even though 16 K points are needed to define the QCPMG decay, simulations of this experiment for pulse spacing $2\tau \leqslant 400$ μs are more efficient than either static line shapes or MAS.

Fig. 15 shows line shapes for all three experiments. In this slow motion regime, the jump rate has virtually no effect on the static line shape (bottom trace). Unlike the situation for deuterons, MAS with 2nd order quadrupole coupling (middle trace) still has enough residual quadrupole broadening to obscure contributions from jumps at rates below about 1000 s^{-1}. However, the MAS line widths are narrow enough in Fig. 15 that spectra for the center bands of the two sites are completely resolved. For both sites, the isotropic second order quadrupole shift computed by EXPRESS agrees with the analytic result for no exchange, $\delta_{iso}^{(2Q)} = -45\omega_Q^2(1+\eta^2/3)/10\omega_0 = -5.4$ kHz. The center band for site 2 is shifted up field from this position by δ_{iso} = 109.3 MHz × 100 ppm = 10.9 kHz. The spin rate 25 kHz is fast enough to suppress contributions from chemical shift anisotropy. Again unlike the situation for deuterons, the central transition for half-integer spin $I > 1$ behaves like a pseudo spin 1/2 system, so the 180° pulses in the QCPMG pulse train refocus both $\delta_{1\Sigma O}$ and $\delta_{iso}^{(2Q)}$. This leads to a complex set of overlapping side bands (upper trace), but the side band line widths, which unlike MAS are free from second order quadrupole broadening, do provide useful dynamic information about the slow jump rate.

Before leaping to the conclusion that QCPMG is superior to MAS for investigating slow dynamics of high spin quadrupolar nuclei, it is necessary to consider the influence of pulse spacing on the side band line widths. Fig. 16 shows QCPMG spectra simulated for pulse spacings between 20 and 200 μs. It is apparent that the side band line widths are anisotropic, strongly dependent on pulse spacing, and decrease noticeably for pulse spacings shorter than ~50 μs. For small pulse spacings, the site-specific coherences do not have enough time to accumulate significant phase before the next refocusing pulse arrives. Thus, random jumps no longer result in loss of phase coherence. This "spin locking" effect is entirely analogous to that observed for liquid state CPMG measurements of exchange among chemically shifted sites [78]. However, unlike the situation for isotropic liquids, no completely analytic solution for the solid state QCPMG line widths is possible (even for two-site exchange) because for any given jump rate, some of the crystallites will exhibit small enough splitting to be in the fast motion limit while others will not [30]. Thus, analysis of the QCPMG line widths requires a complete simulation. Despite this complication, as well as the need to account for orientation-dependent, underlying homogeneous line widths, it appears that QCPMG experiments offer significant advantages over MAS for investigating dynamics of high spin quadrupolar nuclei.

5. Conclusions and prognosis

EXPRESS is an efficient, platform-independent program for simulating effects of jump dynamics on multiple time scales for a wide variety of solid state NMR experiments, including investigations of high spin quadrupolar nuclei as well as deuterons. For complex motion on multiple time scales, EXPRESS provides a useful interface for limiting the number of adjustable parameters to a manageable number. For example, the code is sufficiently efficient that small angle, restricted diffusive motion can effectively be modeled using the formulation of Nadler and Shulten [62]. Simulations of magic angle spinning experiments are shown to be surprisingly efficient compared to those for wide line shapes of stationary samples, and the general conclusion for deuterons is that MAS is superior in most respects to static quadrupole echo experiments. EXPRESS can simulate effects of jump dynamics on deuteron T_{1Z} and T_{1Q} experiments. It is shown that motions too slow to affect the line shape directly can profitably be studied via their tendency to partially average relaxation time anisotropy produced by faster motions. EXPRESS simulations of jump-dynamic effects on spectra of high spin quadrupolar nuclei graphically demonstrate the limitations of the semiclassical formulation of this problem, and they also show that QCPMG experiments on high spin quadrupoles may be more useful than MAS for quantitative studies of dynamics. Source code and documentation for EXPRESS is available on our web site, http://www.wm.edu/nmr.

Acknowledgments

This work was supported by the National Science Foundation, Grant CHE-0713819. We are grateful to Liliya Vugmeyster and Dimitri Ostrovsky for extensive, painstaking assistance in testing preliminary versions of EXPRESS.

References

[1] H.W. Spiess, R. Grosescu, U. Haeberlen, Chem. Phys. 6 (1974) 226.
[2] R.G. Griffin, Methods Enzymol. 72 (1981) 108.
[3] D.M. Rice, R.J. Wittebort, R.G. Griffin, E. Meirovitch, E.R. Stimson, Y.C. Meinwald, J.H. Freed, H.A. Scheraga, J. Am. Chem. Soc. 103 (1981) 7707.
[4] H.W. Spiess, Colloid Polym. Sci. 261 (1983) 193.
[5] J.H. Davis, K.R. Jeffrey, M. Bloom, M.I. Valic, T.P. Higgs, Chem. Phys. Lett. 42 (1976) 390.
[6] N. Boden, L.D. Clark, S.M. Hanlon, M. Mortimer, Faraday Symp. Chem. Soc. 1979 (1978) 109.
[7] J. Jeener, P. Broekaert, Phys. Rev. 157 (1967) 232.
[8] H.W. Spiess, J. Chem. Phys. 72 (1980) 6755.
[9] S.B. Ahmad, K.J. Packer, Mol. Phys. 37 (1979) 47.
[10] R.L. Vold, W.H. Dickerson, R.R. Vold, J. Magn. Reson. 43 (1981) 213.
[11] A. Schmidt, S.O. Smith, D.P. Raleigh, J.E. Roberts, R.G. Griffin, S. Vega, J. Chem. Phys. 85 (1986) 4248.
[12] M.J. Duer, M.H. Levitt, Solid State Nucl. Magn. Reson. 1 (4) (1992) 211.
[13] J.H. Kristensen, H. Bildsoe, H.J. Jakobsen, N.C. Nielsen, J. Magn. Reson. 100 (1992) 437.
[14] P. Hazendonk, A.D. Bain, H. Grondey, P.H.M. Harrison, R.S. Dumont, J. Magn. Reson. 146 (2000) 33.
[15] Y. Huang, R.L. Vold, G.L. Hoatson, J. Chem. Phys. 124 (2005) 104504.
[16] R.W. Shurko, S. Wi, L. Frydman, J. Phys. Chem. A 106 (2002) 51.
[17] M. Kotecha, S. Chaudhuri, C.P. Grey, L. Frydman, J. Am. Chem. Soc. 127 (2005) 16701.
[18] J.H. Freed, J. Chem. Phys. 66 (1977) 4183.
[19] E. Meirovitch, J.H. Freed, J. Phys. Chem. 84 (1980) 2459.
[20] G. Moro, J.H. Freed, J. Phys. Chem. 84 (1980) 2837.
[21] A. Ferrarini, P.L. Nordio, G.J. Moro, R.H. Crepeau, J.H. Freed, J. Chem. Phys. 91 (1989) 5707.
[22] E. Meirovitch, Y.E. Shapiro, A. Polimeno, J.H. Freed, J. Phys. Chem. A 110 (2006) 8366.
[23] M.S. Greenfield, A.D. Ronemus, R.L. Vold, R.R. Vold, P.D. Ellis, T.E. Raidy, J. Magn. Reson. 72 (1987) 89.
[24] R.J. Wittebort, E.T. Olejniczak, R.G. Griffin, J. Chem. Phys. 86 (1987) 5411.
[25] R.G. Griffin, K. Beshah, R. Ebelhauser, T.H. Huang, E.T. Olejniczak, D.M. Rice, D.J. Siminovitch, R.J. Wittebort, NATO ASI C228 (1988) 81.
[26] R.R. Vold, R.L. Vold, Adv. Magn. Optic. Reson. 16 (1991) 85.
[27] T.Y. Tse, G.L. Hoatson, R.L. Vold, in: 33rd Experimental NMR Conference Asilomar, CA, 1992.

[28] G.L. Hoatson, R.L. Vold, in: B. Bluemich (Guest Ed.), NMR: Basic Principles & Progress, vol. 32, 1994, pp. 1.
[29] A. Schmidt, S. Vega, J. Chem. Phys. 87 (1987) 6895.
[30] A.J. Vega, R. Poupko, Z. Luz, J. Magn. Reson. 83 (1989) 111.
[31] K. Mueller, R. Poupko, Z. Luz, J. Magn. Reson. 93 (1991) 291.
[32] S. Zamir, Z. Luz, R. Poupko, S. Alexander, J. Chem. Phys. 94 (1991) 5927.
[33] D. Reichert, Z. Olender, R. Poupko, H. Zimmerman, Z. Luz, J. Chem. Phys. 98 (1993) 7699.
[34] A.E. Aliev, K.D.M. Harris, Magn. Reson. Chem. 36 (1998) 855.
[35] F. Larsen, J. Magn. Reson. 171 (2004) 293.
[36] M. Cutajar, S.E. Ashbrook, S. Wimperis, Chem. Phys. Lett. 423 (2006) 276.
[37] T.M. Barbara, M.S. Greenfield, R.L. Vold, R.R. Vold, J. Magn. Reson. 69 (1986) 311.
[38] G.L. Hoatson, R.L. Vold, T.Y. Tse, J. Chem. Phys. 100 (1994) 4756.
[39] M.E. Rose, Elementary Theory of Angular Momentum, Wiley & Sons, New York, 1957.
[40] D.M. Brink, G.R. Satchler, Angular Momentum, Oxford University Press, Oxford, 1993.
[41] A.R. Edmonds, Angular Momentum in Quantum Mechanics, Princeton University Press, 1957.
[42] H. Goldstein, Classical Mechanics, Addison Wesley, Cambridge, 1953.
[43] R.R. Ernst, G. Bodenhausen, A. Wokaun, Principles of Nuclear Magnetic Resonance in One and Two Dimensions, Oxford, 1987.
[44] T.P. Das, E.L. Hahn, Nuclear Quadrupole Resonance Spectroscopy, Academic Press, New York, 1958.
[45] M. Duer, Introduction to Solid State NMR Spectroscopy, Blackwell Publishing Ltd., Oxford, UK, 2004.
[46] U. Haeberlen, H.W. Spiess, D. Schweitzer, J. Magn. Reson. 6 (1972) 39.
[47] U. Haeberlen, High Resolution NMR in Solids: Selective Averaging, Academic Press, New York, 1976.
[48] R.K. Harris, E.M. Becker, S.M. Cabral De Menzies, P. Granger, R.E. Hoffman, K.W. Zilm Puer, Appl. Chem. 80 (2008) 59.
[49] M. Goldman, P.J. Grandinetti, A. Llor, Z. Olejniczak, J.R. Sachleben, J.W. Zwanziger, J. Chem. Phys. 97 (1992) 8947.
[50] Z. Zheng, Z. Gan, N.K. Sethi, D.W. Alderman, D.M. Grant, J. Magn. Reson. 95 (1991) 509.
[51] T. Charpentier, C. Fermon, J. Virlet, J. Chem. Phys. 109 (8) (1998) 3116.
[52] D.H. Zhou, G.L. Hoatson, R.L. Vold, J. Magn. Res. 167 (2004) 242.
[53] J. Van Kranendonk, Physica 20 (1954) 781.
[54] M. Eden, M.H. Levitt, J. Magn. Reson. 132 (1998) 220.
[55] S.K. Zaremba, Ann. Mate. Pure Appl. 73 (1966) 293.
[56] V.B. Cheng, H.H. Suzukawa, M. Wolfsberg, J. Chem. Phys. 59 (1973) 3992.
[57] A. Abragam, Principles of Nuclear Magnetism, Clarendon Press, Oxford, 1961.
[58] H.M. McConnell, J. Chem. Phys. 28 (3) (1958) 430.
[59] A. Schmidt, S. Vega, J. Chem. Phys. 96 (1992) 2655.
[60] M.H. Levitt, L. Di Bari, Phys. Rev. Lett. 69 (1992) 3124.
[61] G.A. Meints, P.A. Miller, K. Pederson, Z. Shajani, G. Drobny, J. Am. Chem. Soc. 130 (23) (2008) 7305.
[62] W. Nadler, K. Shulten, J. Chem. Phys. 84 (1986) 4015.
[63] D.A. Torchia, A. Szabo, J. Magn. Reson. 49 (1982) 107.
[64] M.S. Solum, K.W. Zilm, J. Michl, D.M. Grant, J. Phys. Chem. 87 (1983) 2940.
[65] M.J. Brown, G.L. Hoatson, R.L. Vold, Solid State NMR 6 (1996) 167.
[66] G.L. Hoatson, R.L. Vold, in: D.M. Grant, R.K. Harris (Eds.), Encyclopedia of Nuclear Magnetic Resonance, vol. 3, Wiley & Sons Scientific, 1995, p. 1582.
[67] F.H. Larsen, H.J. Jakobsen, P.D. Ellis, N.C. Nielsen, Chem. Phys. Lett. 292 (1998) 467.
[68] J.C. Williams, A. McDermott, J. Phys. Chem. 97 (1993) 12393.
[69] N.J. Heaton, R.L. Vold, R.R. Vold, J. Am. Chem. Soc. 111 (1989) 3211.
[70] A.E. Aliev, S.P. Smart, K.D.M. Harris, J. Mater. Chem. 4 (1994) 35.
[71] N.K. Sethi, D.W. Alderman, D.M. Grant, Mol. Phys. 71 (1990) 217.
[72] A. Nayeem, J.P. Yesinowski, J. Chem. Phys. 89 (1988) 4600.
[73] G. Kervern, S. Steurnagel, F. Engleke, G. Pintacuda, L. Emsley, J. Am. Chem. Soc. 129 (2007) 14118.
[74] J.H. Kristensen, I. Farnan, J. Chem. Phys. 114 (2001) 9608.
[75] T. Vießhaus, T. Bolse, K. Müller, Solid State Ionics 177 (35–36) (2006) 3063.
[76] M.I. Gordon, M.J.R. Hoch, J. Phys. C 11 (1978) 783.
[77] O.B. Lapina, D.F. Khabibulin, K.V. Romanenko, Z. Gan, M.G. Zuev, V.N. Krasil'nikov, V.E. Fedorov, Solid State NMR 28 (2005) 204.
[78] H.S. Gutowsky, R.L. Vold, E.J. Wells, J. Chem. Phys. 43 (1967) 4107.